IDEAL COMPLIANT JOINTS AND INTEGRATION OF COMPUTER AIDED DESIGN AND ANALYSIS

Ashraf M. Hamed[1]
Paramsothy Jayakumar[2]
Michael D. Letherwood[2]
David J. Gorsich[2]
Antonio M. Recuero[1]
Ahmed A. Shabana[1]

[1]Department of Mechanical and Industrial Engineering, University of Illinois at Chicago, 842 West Taylor Street, Chicago, IL 60607.
[2]U.S. Army RDECOM-TARDEC, 6501 E. 11 Mile Road, Warren, MI 48397-5000.

Report Documentation Page

Form Approved
OMB No. 0704-0188

1. REPORT DATE	2. REPORT TYPE	3. DATES COVERED
17 NOV 2013	**Technical Report**	**08-03-2012 to 18-08-2013**

4. TITLE AND SUBTITLE	5a. CONTRACT NUMBER
IDEAL COMPLIANT JOINTS AND INTEGRATION OF COMPUTER AIDED DESIGN AND ANALYSIS	**W911NF-07-D-0001**
	5b. GRANT NUMBER
	5c. PROGRAM ELEMENT NUMBER
6. AUTHOR(S)	5d. PROJECT NUMBER
Ashraf Hamed; Paramsothy Jayakumar; Michael Letherwood; David Gorsich; Abtibui Recuero	5e. TASK NUMBER
	5f. WORK UNIT NUMBER
7. PERFORMING ORGANIZATION NAME(S) AND ADDRESS(ES)	8. PERFORMING ORGANIZATION REPORT NUMBER
university of Illinois,842 West Taylor Street,Department of Mechanical and Industrial Engineering,Chicago,IL,60607	**; #24314**
9. SPONSORING/MONITORING AGENCY NAME(S) AND ADDRESS(ES)	10. SPONSOR/MONITOR'S ACRONYM(S)
U.S. Army TARDEC, 6501 East Eleven Mile Rd, Warren, Mi, 48397-5000	**TARDEC**
	11. SPONSOR/MONITOR'S REPORT NUMBER(S)
	#24314

12. DISTRIBUTION/AVAILABILITY STATEMENT

Approved for public release; distribution unlimited

13. SUPPLEMENTARY NOTES

14. ABSTRACT

This paper discusses fundamental issues related to the integration of computer aided design and analysis (I-CAD-A) by introducing a new class of ideal compliant joints that account for the distributed inertia and elasticity. The absolute nodal coordinate formulation (ANCF) degrees of freedom are used in order to capture modes of deformation that cannot be captured using existing formulations. The ideal compliant joints developed can be formulated, for the most part, using linear algebraic equations, allowing for the elimination of the dependent variables at a preprocessing stage, thereby significantly reducing the problem dimension and array storage needed. Furthermore, the constraint equations are automatically satisfied at the position, velocity, and acceleration levels. When using the proposed approach to model large scale chain systems, differences in computational efficiency between the augmented formulation and the recursive methods are eliminated, and the CPU times resulting from the use of the two formulations become similar regardless of the complexity of the system. The elimination of the joint constraint equations and the associated dependent variables also contribute to the solution of a fundamental singularity problem encountered in the analysis of closed loop chains and mechanisms by eliminating the need to repeatedly change the chain or mechanism independent coordinates. It is shown that the concept of the knot multiplicity used in computational geometry methods, such as B-spline and NURBS (Non-Uniform Rational B-Spline), to control the degree of continuity at the breakpoints is not suited for the formulation of many ideal compliant joints. As explained in this paper, this issue is closely related to the inability of B-spline and NURBS to model structural discontinuities. Another contribution of this paper is demonstrating that large deformation ANCF finite elements can be effective, in some MBS application, in solving small deformation problems. This is demonstrated using a heavily constrained tracked vehicle with flexible link chains. Without using the proposed approach, modeling such a complex system with flexible links can be very challenging. The analysis presented in this paper also demonstrates that adding significant model details does not necessarily imply increasing the complexity of the MBS algorithm.

15. SUBJECT TERMS

Compliant joints; tracked vehicle; flexible multibody systems; finite element; ANCF; closed loop chains; I-CAD-A

16. SECURITY CLASSIFICATION OF:			17. LIMITATION OF ABSTRACT	18. NUMBER OF PAGES	19a. NAME OF RESPONSIBLE PERSON
a. REPORT	b. ABSTRACT	c. THIS PAGE			
unclassified	**unclassified**	**unclassified**	**Public Release**	**53**	

ABSTRACT

This paper discusses fundamental issues related to the integration of *computer aided design and analysis* (I-CAD-A) by introducing a new class of *ideal compliant joints* that account for the distributed inertia and elasticity. The *absolute nodal coordinate formulation* (ANCF) degrees of freedom are used in order to capture modes of deformation that cannot be captured using existing formulations. *The ideal compliant joints* developed can be formulated, for the most part, using linear algebraic equations, allowing for the elimination of the dependent variables at a preprocessing stage, thereby significantly reducing the problem dimension and array storage needed. Furthermore, the constraint equations are automatically satisfied at the position, velocity, and acceleration levels. When using the proposed approach to model large scale chain systems, differences in computational efficiency between the augmented formulation and the recursive methods are eliminated, and the CPU times resulting from the use of the two formulations become similar regardless of the complexity of the system. The elimination of the joint constraint equations and the associated dependent variables also contribute to the solution of a fundamental singularity problem encountered in the analysis of closed loop chains and mechanisms by eliminating the need to repeatedly change the chain or mechanism independent coordinates. It is shown that the concept of the knot multiplicity used in computational geometry methods, such as B-spline and NURBS (**N**on-**U**niform **R**ational **B**-**S**pline), to control the degree of continuity at the breakpoints is not suited for the formulation of many ideal compliant joints. As explained in this paper, this issue is closely related to the inability of B-spline and NURBS to model structural discontinuities. Another contribution of this paper is demonstrating that large deformation ANCF finite elements can be effective, in some MBS application, in solving small deformation problems. This is demonstrated using a heavily constrained tracked vehicle with flexible link chains. Without using the proposed approach, modeling such a complex system with flexible links can be very challenging. The analysis presented in this paper also demonstrates that adding significant model details does not necessarily imply increasing the complexity of the MBS algorithm.

Keywords: Compliant joints; tracked vehicle; flexible multibody systems; finite element; ANCF; closed loop chains; I-CAD-A

1. INTRODUCTION

Complex multibody systems (MBS) consist of many components connected by mechanical joints. These joints can be modeled using different formulations that lead to different dynamic models. One method for representing mechanical joints in computational MBS algorithms is the *ideal joint formulation*, in which a set of nonlinear algebraic constraint equations are used to define the body connectivity conditions. This approach, when used with existing MBS rigid body formulations or flexible body formulations based on the floating frame of reference (FFR) formulation, does not account for the joint flexibility. Furthermore, in these existing MBS formulations, the joint constraints introduce nonlinearities both in the inertia and constraint forces. Another problem that must be addressed when constrained MBS dynamics algorithms are developed is the violation of the joint kinematic constraints that must be satisfied at the position, velocity, and acceleration levels. This paper proposes a new procedure to address the following fundamental issues:

1. The paper develops a new class of ideal joints that account for the distributed inertia and elasticity at the joint definition point. Additional degrees of freedom are introduced in order to capture modes of deformation that cannot be captured using existing formulations that employ rigid triads or unit vectors to formulate the joint equations.
2. The ideal compliant joints developed in this paper, while more general and capture more modes of displacements, can be, for the most part, formulated using linear algebraic equations. These linear connectivity conditions allow for the elimination of the dependent variables at a preprocessing stage, thereby significantly reducing the problem dimension and array storage needed.

3. Because linear connectivity conditions are used to eliminate the dependent variables at a preprocessing stage, the constraint equations are automatically satisfied at the position, velocity, and acceleration levels. Therefore, when using the proposed approach to model large scale chain systems, differences in computational efficiency between the augmented formulation and the recursive methods are eliminated, and the CPU times resulting from the use of the two formulations become similar regardless of the complexity of the system.
4. Furthermore, the elimination of the joint constraint equations and the associated dependent variables contribute to the solution of a fundamental singularity problem encountered in the analysis of closed loop chains and mechanisms. It is known that in the case of closed loop chains and mechanisms, the set of independent coordinates must be repeatedly changed in order to avoid singularity of the constraint Jacobian matrix. This problem can be avoided by using the new ANCF finite element meshes that allow for the elimination of the constraint equations and the dependent variables at a preprocessing stage.
5. Using the concept of the ideal compliant joints, the fundamental problems that can be encountered when using computational geometry methods, such as B-spline and NURBS, as analysis tools are explained. The concept of the *knot multiplicity* used in computational geometry methods does not lend itself easily to the formulation of the ideal compliant joints that may require different degrees of continuity for different variables or elements of the gradient vectors or may require constraints on the gradient vectors along directions that differ from the B-spline and NURBS coordinate lines. This issue is closely related to the inability of B-spline and NURBS to model *structural discontinuities*.

6. While small deformation MBS problems can be effectively solved using the FFR approach that allows for filtering out high frequency contents, there are small deformation problems that can be solved more efficiently using large deformation formulation such as the absolute nodal coordinate formulation (ANCF). In these small deformation problems, the inclusion of high frequency modes may be necessary. An example of these problems is a flexible-link chain of a tracked vehicle where each link is modeled using one finite element only. The use of ANCF finite elements can be advantageous as compared to the use of the FFR formulation. This important issue is addressed in this paper.
7. The necessity of using the new concepts developed in this paper in modeling complex systems is demonstrated using a heavily constrained tracked vehicle with flexible-link chains. Without using the proposed approach modeling such a complex system with flexible links can be very challenging.

The analysis presented in this paper demonstrates that adding significant model details does not necessarily imply increasing the complexity of the MBS algorithm. In fact, including significant details such as body flexibility and joint deformations can be accomplished using MBS algorithms that are much simpler than the algorithms currently used for rigid body system analysis. This can be achieved using the ANCF finite elements that lead to new meshes that have linear connectivity and constant inertia. By using the geometry concepts that allow for successful integration of computer aided design and analysis (I-CAD-A) and using the new ANCF meshes to model heavily constrained systems such as long chains, the distinction between the augmented and recursive methods can be eliminated.

2. BACKGROUND

Several FE/MBS , formulations have been developed for the deformation analysis of mechanical systems. Some of these formulations are suited for the analysis of large rotation small deformation problems, while the others can be used in the analysis of large rotation and large deformation problems. An example of the large rotation and small deformation formulation is the FE/FFR formulation which employs mixed set of reference and elastic coordinates (Shabana, 2014). This formulation leads to a highly nonlinear inertia matrix that has a strong coupling between the reference and deformation coordinates. In addition to the high nonlinearity of the inertia forces, the joint constraints equations developed using the FFR formulation are also highly nonlinear because of the use of orientation parameters (Korkealaakso et al, 2009). Furthermore, rigid triads and unit vectors are often used in the formulation of the joints in the rigid body and FFR algorithms, and as a result, these ideal joint formulations do not capture modes of deformation.

While the FFR formulation will remain an effective approach for modeling small deformation problems because it allows for filtering out high frequency modes, the more general large rotation large deformation finite element *absolute nodal coordinate formulation* (ANCF) can be effective in solving a class of small deformation problems (Shabana et al, 2012; Hamed et al, 2011; Shabana, 2010, 2012; Dimtrochenko and Pogorelov, 2003; Abbas et al, 2010; Dufva et al, 2005, 2007; Schwab and Meijaard, 2010; Shabana and Mikkola, 2003; Tian et al, 2009; Yakoub and Shabana, 2001; Omar and Shabana, 2001). ANCF finite elements can be used to model both structural and nonstructural discontinuities in a straightforward manner (Shabana et al, 2012; Hamed et al, 2011). Using ANCF finite elements, the absolute position vectors and their gradients are considered nodal coordinates. The global position of an arbitrary point on an

element *k* of body *i* can be defined in a global coordinate system as $\mathbf{r}^{ik} = \mathbf{S}^{ik}(x^{ik}, y^{ik}, z^{ik})\mathbf{e}^{ik}(t)$, where $\mathbf{S}^{ik}(x^{ik}, y^{ik}, z^{ik})$ is the space-dependent matrix that defines the element shape functions, and $\mathbf{e}^{ik}$ is time-dependent vector of nodal coordinates. An example of ANCF finite elements is the three-dimensional gradient deficient Euler-Bernoulli beam element shown in Fig. 1. For this element, the vector of nodal coordinates $\mathbf{e}^{ik}$, which contains position and position gradient vectors, can be defined as $\mathbf{e}^{ik} = \left[\mathbf{r}^{ik1\mathrm{T}} \;\; \frac{\partial \mathbf{r}^{ik1\mathrm{T}}}{\partial x^{ik}} \;\; \mathbf{r}^{ik2\mathrm{T}} \;\; \frac{\partial \mathbf{r}^{ik2\mathrm{T}}}{\partial x^{ik}} \right]^{\mathrm{T}}$ (Gerstmayr and Shabana, 2006; Shabana, 2012), where $\mathbf{r}^{ikj}$ and $\left(\partial \mathbf{r}^{ikj} / \partial x^{ik}\right)$ refer to the displacement and displacement gradient vectors at node *j* of element *k*. While ANCF finite elements were introduced for large deformation problems of very flexible bodies, these elements can be very effective in the analysis of small deformation in complex flexible multibody systems containing a large number of joints and flexible links. As demonstrated in this paper using a large scale tracked vehicle that has flexible-link chains, ANCF finite elements can be used to capture model details that cannot be captured using small deformation and rigid body formulations.

A number of approaches have been proposed in the literature for developing tracked vehicle models. Galaitsis (1984) introduced a comprehensive model incorporating the dynamics of independent rigid track shoes. In this model, the equations of motion for the track chain were developed for a tracked vehicle traveling on a flat ground. Bando et al (1991) developed a procedure for the design and analysis of small-size rubber tracked bulldozers. They presented a computer simulation which was used in the evaluation of the vehicle behavior. Nakanishi and Shabana (1994) introduced a model for the nonlinear dynamic analysis of two dimensional tracked vehicle systems. They used both the augmented and the velocity transformation techniques. In their investigation, it was shown that the singularity problem, which can be

encountered if one set of independent coordinates is used throughout the simulation, can be avoided by either repeatedly changing the set of independent coordinates or by using a penalty function approach. In this latter approach, a cut is made at a selected secondary joint in the track in order to form an open loop structure, and the chain is closed using a spring with high stiffness coefficient. Choi et al (1998A; 1998B) developed a three dimensional contact force model that represents the interaction between the track links and the vehicle components. In their work, track links were connected using perfect pin joints. The highly nonlinear joints constraint equations were adjoined to the equations of motion using the augmented formulation. Maqueda et al (2010) developed a three-dimensional tracked vehicle model with rubber chains modeled using ANCF finite elements which allows for a straightforward implementation of general linear and nonlinear material models. The cross section deformation results obtained using ANCF finite elements were validated by comparing with the results obtained using solid finite elements in the case of a simple tension test. In previous investigations (Hamed et al, 2011; Shabana et al, 2012), an ANCF C^0/C^1 continuity flexible-link chain mesh was developed. This new ANCF mesh can be used in the efficient modeling of flexible-link chains. The C^0/C^1 ANCF chain model leads to linear connectivity conditions, thereby allowing for an efficient elimination of the dependent joint variables at a preprocessing stage. Using this approach, the ANCF mesh mass matrix remains constant in the case of articulated systems.

The organization of this paper is as follows. Section 3 discusses the problems of large rotation and slope discontinuities in MBS dynamics. In Section 4, a brief review of the recently developed linear finite element ANCF meshes that have linear connectivity conditions and constant inertia matrix is presented. This section also proposes a new simple model for the sliding joint. Section 5 discusses some of the limitations of the B-spline representation when

flexible-link chain structures are considered. Control points used in the B-spline representation may not represent material points, leading to some fundamental issues that are discussed in Section 5. The discussion presented in Section 5 sheds light on the potential of using ANCF as the basis for the *integration of computer aided design and analysis* (I-CAD-A). Section 6 provides a justification for the use of ANCF finite elements to model complex flexible-link chains. Section 7 describes the simplified three-dimensional Euler-Bernoulli beam elastic force model used to demonstrate the procedures and concepts introduced in this study. In Section 8, a tracked vehicle model is used to obtain the numerical results that demonstrate the potential of using the new ANCF meshes in capturing model details that cannot be captured using existing methods. Summary and conclusions drawn from this study are presented in Section 9.

3. STRUCTURAL AND NONSTRUCTURAL DISCONTINUITIES

Structural and nonstructural discontinuities have been fundamental issues in the development of MBS formulations. Understanding these types of discontinuities will also shed light on the fundamental differences between the approaches currently being developed for the integration of computer aided design and analysis. Structural discontinuities refer to the type of joints that do not allow relative rigid body displacements, while nonstructural discontinuities refer to the types of joints that allow for relative rigid body displacements. The joints used in flexible-link chains are example of joints that lead to nonstructural discontinuities.

Structural discontinuity was the main issue in the development of the large displacement small deformation FE/FFR formulation. In the classical finite element formulations, beams, plates, and shells, which employ infinitesimal rotations as nodal coordinates, are considered nonisoparametric elements. Rigid body motion of such elements does not lead to zero strains and rigid body inertia cannot, in general, be exactly modeled (Shabana, 2014). Therefore, before

introducing the FE/FFR formulation in the early eighties, an incremental approach was needed when these elements are used in the analysis of large rotation problems. Because the incremental solution of linearized system of equations eventually deviates from correct solution, there was a need to develop a new FE formulation that correctly describes rigid body motion when nonisoparametric elements are used. For this reason, the FFR formulation was introduced. In this formulation, a floating body coordinate system which shares the large displacement and rotation of the body is introduced. The large displacement of the body can be described using the global position of the floating frame origin and a set of orientation parameters that can be used to define the FFR transformation matrix. The use of these independent *reference coordinate*s is sufficient to describe correctly the rigid body motion. Nonetheless, the introduced body coordinate system, if not used with the finite element method, allows only modeling simple geometries that do not have any slope discontinuities as the one shown in Fig. 2. On the other hand, complex geometries that consist of elements with different orientations as shown in Fig. 3 can be modeled using the concept of the *intermediate element coordinate system*. This coordinate system has an origin that is rigidly attached to the origin of the body coordinate system and has axes that are initially parallel to the axes of the finite element coordinate system as shown in Fig. 4. Using this coordinate system, the finite elements that have different orientations can be connected rigidly using linear algebraic constraint equations at a preprocessing stage. Therefore, the FE/FFR formulation provides a general solution for accurately modeling structural geometric discontinuities using linear connectivity conditions. This leads to an FE mesh that is locally linear allowing for the use of coordinate reduction techniques to filter out high frequency modes of vibration.

Another type of slope discontinuity is the nonstructural discontinuity which permits the relative rigid body displacements between the segments connected. Example of which is a chain of links connected by pin joints as the one shown in Fig. 5. In the case of large relative rotation between the connected links, the dynamics of these chains, even for a planar rigid-link chain, is governed by highly nonlinear equations as the result of the geometric nonlinearities due to the finite relative rotations (Korkealaakso et al, 2009). For this type of joints, the FFR or rigid body formulations lead to a highly nonlinear connectivity conditions as the result of using orientation parameters. Furthermore, the resulting joint formulations do not include any deformation modes since the resulting joint degrees of freedom define only relative rigid body displacements.

A systematic approach for modeling joints between flexible bodies using ANCF finite elements was introduced by Sugiyama et al (2003). In their work, tangent frames were used to define transformation matrices at the joint definition points. This approach leads to complex nonlinear constraints that are adjoined to the system equations of motion using the technique of Lagrange multipliers. Nonetheless, as demonstrated in previous publications, a linear finite element mesh of chains that consist of flexible links can be developed in many MBS applications (Vallejo et al., 2003; Hamed et al, 2011; Shabana et al, 2012). This can be achieved using ANCF finite elements which allow for developing an FE mesh that includes one or more chains with flexible links, and each of the links can have independent relative finite rotations. The connectivity conditions between the ANCF finite elements can be described using linear algebraic constraint equations that can be used at a preprocessing stage to eliminate redundant variables. The use of this new concept can lead to significant simplification of the MBS algorithm and can eliminate the distinction between the augmented and recursive methods. Both the augmented and recursive methods will converge to approximately the same CPU time. Figure

6 shows two flow charts that describe the steps of the dynamic analysis of two different ANCF chains defined using the conventional nonlinear constraint approach and the new linear ANCF constraint approach. It is clear that using the new ANCF linear constraint approach is more efficient since it eliminates many of the time-consuming steps of the conventional approach. For instance, when the new approach is used, there is no need to solve the constraint equations at the position, velocity or acceleration levels. Furthermore, the dimension of the system differential/algebraic equations will be significantly reduced as a result of the elimination of dependent variables and the associated Lagrange multipliers.

4. ANCF JOINT FORMULATIONS AND DEFORMATION MODES

Using ANCF finite elements, mechanical joints between finite elements can be formulated using linear connectivity conditions (Vallejo et al., 2003; Hamed et al, 2011; Shabana et al, 2012). This is an important feature that can be exploited to significantly reduce the number of nonlinear algebraic constraint equations and the associated Lagrange multipliers in many MBS applications. Several flexible bodies can be modeled as one FE mesh consisting of elements that have relative translations and finite rotations with respect to each other. It is demonstrated in this section, using several examples, how the linear joint equations can be developed and how ANCF finite elements can also reduce the degree of nonlinearity when linear joint formulations cannot be obtained for some joints. The modes of the deformation of the new ANCF joints are also discussed in this section.

4.1. Spherical Joint

When two bodies or finite elements are connected by a spherical joint, one has C^0 continuity that ensures only the continuity of the position coordinates. The two connected bodies can

arbitrarily rotate with respect to each other. For a spherical joint between two finite elements i and j, the algebraic spherical joint constraint equations can be written as

$$\mathbf{r}^{i,B} = \mathbf{r}^{j,A}, \tag{1}$$

where *A* and *B* refer to the joint node on the finite elements *i* and *j*, respectively. The preceding constraint equations eliminate the relative translation between the two finite elements. However, since ANCF structural finite elements can correctly describe arbitrary rigid body rotations, applying the linear algebraic equations of Eq. 1 at a preprocessing stage allows for developing a FE mesh in which each finite element can have an independent rotational displacement. Note that the above spherical joint constraints are linear in the ANCF coordinates. The same constraint equations are highly nonlinear in the case of the rigid body or the FFR formulation (Shabana, 2001).

4.2. Pin Joint

The formulation of the three-dimensional ANCF linear pin joint will be discussed using two different ANCF finite elements. The first element is the three-dimensional Euler-Bernoulli beam element. This element has only one gradient vector tangent to the element center line. In order for two three-dimensional ANCF Euler-Bernoulli finite elements to be connected by a pin joint, two sets of conditions must be satisfied. The first set of conditions is the continuity of the position coordinates at the joint definition point. This set of conditions can be imposed at a preprocessing stage by using the same position degrees of freedom for the two elements at the joint node. The second set of conditions constrain the normals to the gradient vectors at the joint point to be parallel to each other. This second set of conditions can also be introduced at a preprocessing stage by applying continuity on the component of the gradient vector in the

direction of the joint axis. The constraint equations of a pin joint between two ANCF Euler-Bernoulli beam elements *i* and *j* can thus be written as follows:

$$\mathbf{r}^{i,B} = \mathbf{r}^{j,A}, \quad \left(\frac{\partial \mathbf{r}^{i,B}}{\partial x}\right)_{\alpha} = \left(\frac{\partial \mathbf{r}^{j,A}}{\partial x}\right)_{\alpha}, \tag{2}$$

where $\alpha = 1, 2, \text{or } 3$ denotes the direction of the joint axis. The preceding equations represent a set of four scalar equations. The second equation in Eq. 2 is a scalar equation that equates the α th component of element i gradient vector along the joint axis to the corresponding α th component of element j gradient vector. For example, if the joint axis is the element y axis, then in this case $\alpha = 2$. Note that the second set of algebraic equations can be formulated at a preprocessing step and can be used to eliminate dependent variables before the start of the dynamic simulation. Using the preceding equations, one can develop one linear FE mesh for flexible-link mechanisms in which the links can have arbitrarily large relative rotations and large deformations without the need to include nonlinear algebraic constraint equations in the formulation since these conditions can be eliminated as a preprocessing stage. Note that for the gradient deficient Euler-Bernoulli beam element, the joint axis needs to be one of the finite element axes in order to obtain the linear relationships of Eq. 2. This restriction, which can be relaxed when using fully parameterized ANCF finite elements, does not represent a serious limitation when chain models are developed.

Another example of ANCF finite elements is the three-dimensional shear deformable beam element. A node on this fully parameterized ANCF element has 12 degrees of freedom. These degrees of freedom include three rigid body translations, three rotations, and six deformation modes. One may introduce a pin joint formulation that uses the following six scalar equations defined at the joint node between elements *i* and *j* (Shabana et al, 2012).

$$\mathbf{r}^{i,B} = \mathbf{r}^{j,A} \quad , \quad \frac{\partial \mathbf{r}^{i,B}}{\partial \beta} = \frac{\partial \mathbf{r}^{j,A}}{\partial \beta} . \tag{3}$$

In the above equations, β is the coordinate that defines the joint axis. It can be either *x, y, z,* or any other coordinate line since the use of ANCF finite elements allows for a straight forward application of the gradient tensor transformation. The six scalar equations represented by Eq. 3 define a pin joint with six degrees of freedom: one rotation and five deformation degrees of freedom. Consequently, the joint leads to C^1 continuity for the gradient vector along the coordinate line β and C^0 continuity for the remaining gradient vectors.

4.3. Sliding Joint

Sliding joints between flexible bodies are examples of variable boundary conditions joints. Developing the kinematic equations of these joints using the FFR formulation that employs linear modes can be difficult because the change of the boundary conditions. On the other hand, these joints can be systematically formulated using ANCF finite elements as explained in the literature (Sugiyama et al, 2003). Using ANCF finite elements, a procedure was introduced to model the sliding joints using local frames defined at the joint definition point. A tangent frame can be used to define a joint local coordinate system whose transformation matrix at the joint definition point can be evaluated. In order to define the time derivative of the constraint equations, the time derivatives of the columns of the transformation matrices are written as function of the generalized coordinates and velocities. This procedure leads to complex constraint equations that are difficult to implement. The same joint constraints can be formulated using a simple and straightforward approach by introducing two *nongeneralized coordinates*. The first nongeneralized coordinate *u* defines the local position of the joint definition point on the base element as shown in Fig. 7, while the second one *m* defines the ratio between lengths of

the two element position gradient vectors in the direction of the sliding axis. The following equations can be used to define the constraint equations of the sliding joint:

$$\mathbf{C}(\mathbf{e}^i, \mathbf{e}^j, u^i) = \mathbf{r}_p^i(\mathbf{e}^i, u^i) - \mathbf{r}_p^j(\mathbf{e}^j) = \mathbf{0}, \quad \frac{\partial \mathbf{r}^i}{\partial \zeta} = m \frac{\partial \mathbf{r}^j}{\partial \gamma} \quad . \tag{4}$$

In the above equations, ζ and γ are the coordinate lines in the direction of the joint axis on each element, and, $\mathbf{e}^i$ and $\mathbf{e}^j$ are the nodal coordinates of the two finite elements. These constraint equations can be applied to constrain 4 of the joint degrees of freedom: 2 rigid rotations, and 2 rigid translations. The sliding is ensured by requiring continuity of the gradient along the sliding axis and preventing the joint definition point from moving normal to the direction of the sliding axis. This guarantees the freedom of sliding without the need to define local frames which lead to complex constraint equations required to ensure the parallelism of the sliding axes.

4.4. ANCF Joint Deformation Modes

In rigid body and small deformation FFR MBS algorithms, joint formulations allow for only relative rigid body degrees of freedom that describe the relative displacements between two rigid triads attached to the two bodies connected by the joint. The ANCF joint formulations, on the other hand, allow for deformation modes at the joint definition point. This leads to a new class of *ideal compliant joints* defined using algebraic equations. The gradient vectors of the two elements can change their magnitude and orientation allowing for stretch and shear deformations at the joint node. Depending on the element type and the number of algebraic equations used in the formulation of the joint, different deformation modes can be captured. As an example, the gradient deficient Euler-Bernoulli beam element allows for only the axial, bending, and twist. Therefore, such an element does not capture shear and cross section deformations. On the other hand, the fully parameterized beam element which has a complete set of gradient vectors can be used to capture the change in the cross section due to deformation at the joint node. For the fully

parameterized beam element, the modes of deformations at the joint nodes can be examined using the Green-Lagrange strain tensor $\boldsymbol{\varepsilon}$ which can be written as $\boldsymbol{\varepsilon} = \frac{1}{2}\left(\mathbf{J}^T\mathbf{J} - \mathbf{I}\right)$, where $\mathbf{J}$ is the matrix of position vector gradients, and $\mathbf{I}$ is the identity matrix. Because the strain tensor $\boldsymbol{\varepsilon}$ is symmetric, one can define the strain vector $\boldsymbol{\varepsilon}_v = \left[\varepsilon_{xx} \;\; \varepsilon_{yy} \;\; \varepsilon_{zz} \;\; \varepsilon_{xy} \;\; \varepsilon_{yz} \;\; \varepsilon_{zx}\right]^{\mathrm{T}}$, where ε_{xx}, ε_{yy} and ε_{zz} are the normal strains, and ε_{xy}, ε_{yz} and ε_{zx} are the shear strains. The strain components are continuous inside the element and some of the strain components can be discontinuous at the joint nodes because of the discontinuity of position vector gradients at these nodes. Figure 8 shows some of the deformation modes of the three-dimensional fully parameterized beam element. These modes are the tensile mode, the bending mode, and one of the cross section deformation modes. The tensile mode is a result of changing the magnitude of the gradient $\mathbf{r}_x$ at the joint point. The bending mode is due to the change of the orientation of the gradient vector $\mathbf{r}_x$ with respect to the line connecting the two nodes of the element. Finally, the cross section deformation mode defines the change of the cross section dimensions which is the result of the change in the magnitude of the gradient vectors along the cross section fibers. Furthermore, the second condition of Eq. 3, $\left(\partial\mathbf{r}^{i,B}/\partial\beta\right) = \left(\partial\mathbf{r}^{j,A}/\partial\beta\right)$, allows for the stretch of the joint pin.

5. COMPARISON WITH THE ISOGEOMETRIC APPROACH

Computational geometry methods such as B-spline and NURBS (Non-Uniform Rational B-Splines) use control points as coordinates. The control points do not necessarily represent material points. This is one of the fundamental differences between computational geometry methods and the finite element method. The *isogeometric analysis* is a concept aims at unifying the two fields of *computer aided design* (CAD) and *finite element analysis* (FEA) by using the same basis for the geometry description and analysis (Hughes et al, 2005). This concept, which

has been used in computer science for many years to build physics based models, has recently received attention from the mechanics community. The increasing interest in isogeometric analysis is motivated by the desire to deal with the difficulties and cost associated with the conversion of solid models to FE analysis models. This conversion process leads to distortion of the geometry of the analysis model because existing structural elements such as beams, plates and shells cannot describe correctly arbitrary geometry.

While the use of the isogeometric analysis can be considered as a step in the right direction, the use of computational geometry methods as analysis can lead to fundamental and implementation problems which can be avoided by using ANCF geometry. In this section, some of the limitations of computational geometry methods when used as analysis tools are discussed. The discussion in this section will focus on the limitations associated with the joint formulations which is the subject of this paper.

5.1 B-Spline Surfaces

In this subsection, the B-spline representation is briefly reviewed in order to provide the background required for the discussion that follows in subsequent subsections. B-spline surfaces can be defined in the following parametric form (Piegl and Tiller, 1997):

$$\mathbf{r}(u,v) = \sum_{i=0}^{n}\sum_{j=0}^{m} N_{i,p}(u) N_{j,q}(v) \mathbf{P}_{i,j} \tag{5}$$

where u and v are the parameters, $N_{i,p}(u)$ and $N_{j,q}(v)$ are B-spline basis functions of degree p and q, respectively, and $\mathbf{P}_{i,j}$ are a set of $(n+1)\times(m+1)$ bidirectional control points. The B-spline basis functions $N_{i,p}(u)$ can be defined as

$$\left.\begin{aligned} N_{i,0}(u) &= \begin{cases} 1 & \text{if } u_i \le u < u_{i+1} \\ 0 & \text{otherwise} \end{cases} \\ N_{i,p}(u) &= \frac{u-u_i}{u_{i+p}-u_i} N_{i,p-1}(u) + \frac{u_{i+p+1}-u}{u_{i+p+1}-u_{i+1}} N_{i+1,p-1}(u) \end{aligned}\right\} \tag{6}$$

where $u_{i,}$, $i = 0,1,2,....,n+p+1$ are called the knots, and $u_i \le u_{i+1}$. The vector $\mathbf{U} = \{u_0 \;\; u_1 \;\; ..... \;\; u_{n+p+1}\}$ is called the knot vector. Similar definitions can be introduced for $N_{j,q}(v)$ with another knot vector $\mathbf{V} = \{v_0 \;\; v_1 \;\; ..... \;\; v_{m+p+1}\}$. The knots of B-spline surfaces do not have to be distinct; distinct knots are called breakpoints and define surface segments with non-zero dimensions. The number of the non-distinct knots in $\mathbf{U}$ and $\mathbf{V}$ at a point is referred to as the *knot multiplicity* associated with the parameters u and v, respectively. The degree of continuity at a breakpoint is controlled by the multiplicity of the knots at this point. A decrease in the knot multiplicity by one leads to an increase in the degree of continuity by one. This amounts to automatic elimination of one control point. The concept of the knot multiplicity can lead to fundamental implementation problems when ideal compliant joints are used in MBS algorithms as discussed later in this paper.

5.2 Basis Functions

ANCF geometry does not impose restrictions on the number of basis functions used in the interpolating polynomials. In contrast, B-spline rigid recurrence formula restricts the number of basis functions depending on the degree of the interpolating functions; there is a relationship between the polynomial degree, the number of knots, and the number of control points. If $r+1$ is the number of knots in $\mathbf{U}$ and $s+1$ is the number of knots in $\mathbf{V}$, then in B-spline geometry, one must have

$$r = n + p + 1, \quad s = m + q + 1 \tag{7}$$

Using Eq. 7, one can show that if a cubic interpolation is used for both u and v, as in the case of

a thin plate, the B-spline representation requires 16 control points regardless of whether the shape of deformation of the plate is simple or complex (Shabana et al, 2012). This can be a disadvantage in the analysis since such a geometric representation can unnecessarily increase the dimension of the analysis model and leads to a loss of the flexibility offered by the FE method. As the degree of the polynomial interpolation increases, this drawback of B-spline becomes more serious.

5.3 Knot Multiplicity

In computational geometry methods, a decrease in the knot multiplicity by one leads to elimination of one control point and to an increase in the degree of continuity by one. The knot multiplicity cannot be used to impose continuity condition on only one element of a position vector or a gradient vector. In three-dimensional analysis, a minimum of three scalar equations are automatically imposed when the knot multiplicity is decreased by one. Some ideal compliant joints, as discussed in this paper, may require imposing only one or two algebraic equations to obtain a certain degree of continuity for one or two elements of a position or gradient vector. Such ideal compliant joint constraints cannot be formulated using the rigid B-spline and NURBS knot multiplicity concept.

5.4 Structural Discontinuities

Structural discontinuities, such as T-, L-, and V-sections, which can be thought of as a sudden change in geometry, represent discontinuities in gradients as the result of the discontinuities of the coordinate lines (directions). Modeling this type of discontinuity, which characterizes both mechanical and structural systems, requires the use of gradient transformation which is fundamental in the implementation of the ANCF geometric representation (Hamed et al, 2011). Using C^0 continuity in B-spline analysis is equivalent to having a pin joint in the planar analysis

and to a spherical joint in the spatial analysis. The case of structural discontinuity, which is also of the C^0 type, requires additional algebraic equations in order to eliminate the relative rotation at the joint definition point. Therefore, there are important geometric configurations where the degree of continuity does not change by eliminating degrees of freedom or equivalently control points. These important geometric configurations cannot be covered by the rigid structure of the B-spline and NURBS which relates the number of degrees of freedom or the control points to the degree of continuity (knot multiplicity).

5.5 Sliding Joints

Another important geometric scenario associated with the ideal compliant constraints is the sliding joint. This type of joint requires continuity of the gradients, but not continuity of all position coordinates. In the B-spline representation, C^1 requires first C^0 continuity. As previously discussed, ANCF representation does not require this sequence, and for this reason, such an ANCF representation can be used to model the sliding joint in a straightforward manner. Modeling the same joint using B-spline geometry is not as straight forward: at a given breakpoint, the multiplicity associated with a knot can be used to change the continuity of the derivatives. For example, in the case of cubic interpolation, C^0, C^1, and C^2 conditions correspond, respectively, to knot multiplicity of three, two, and one. Applying higher degree of continuity implies all lower degree continuity. In other words, a knot multiplicity of three which corresponds to C^2 implies C^0 and C^1 continuity. Similarly, applying C^1 implies C^0 continuity. Therefore, B-spline structure does not allow applying continuity on position gradients without position continuity. Therefore, two sliding bodies must be modeled as two separate meshes and additional algebraic constraint equations must be added to guarantee the sliding motion.

6. USE OF ANCF FOR SMALL DEFORMATION PROBLEMS

Chains are used in many important MBS applications, and therefore, it is important to be able to develop efficient and accurate chain models, particularly when the link flexibility is considered. For example, chains are critical in defining the mobility of tracked vehicles that consist of a large number of components interconnected by joints and force elements. The dynamics of such systems are governed by complex relationships as result of the relative motions and joint forces. Furthermore, considering the flexibility of the track links increases the system complexity, model dimension, and degree of nonlinearity. For this reason, it is necessary to carefully select the procedure used to model the flexible links and the joints connecting them in a chain structure.

As previously discussed, an efficient formulation that can be used to model complex chain systems is the ANCF which allows for the elimination of the joint constraint equations at a preprocessing stage, allowing for the elimination of the joint dependent variables before the dynamic simulation starts and leading to a chain mesh that has a constant inertia matrix and zero Coriolis and centrifugal forces. Furthermore, the ANCF geometry description, in contrast to conventional finite elements, is consistent with the descriptions used in computational geometry methods (Lan and Shabana, 2010; Mikkola et al, 2013).

While ANCF allows for the use of a general continuum mechanics approach, special elastic force models can be derived and implemented in ANCF/MBS algorithms for the solution of specific applications. In the case of the tracked vehicle model considered in subsequent sections, the deformation of the track links is small. Nonetheless, the development of FFR model to study the flexible link chain dynamics is not recommended because of the following specific reasons:

1. The FFR formulation leads to a highly nonlinear mass matrix and complex non-zero Coriolis and centrifugal forces. On the other hand, ANCF leads to a constant inertia matrix and zero Coriolis and centrifugal forces. ANCF Cholesky coordinates can be used to obtain an identity generalized inertia matrix, leading to an optimum sparse matrix structure.
2. The FFR formulation leads to highly nonlinear constraint equations for the joints between the chain links. These constraint equations must be satisfied at the position, velocity, and acceleration levels, and as discussed before, contribute to increasing the problem dimensionality and the array storage needed. In the case of flexible-link chains, the overhead can be significant. On the other hand, ANCF finite elements allow for the formulation of linear connectivity conditions, and therefore, the dependent variables can be eliminated systematically at a preprocessing stage. The use of the new ANCF meshes can lead to significant simplification of the solution algorithm and significant reductions in the array storage as previously discussed.
3. In both rigid and FFR chain models, the use of closed chains can lead to singular configurations if one set of independent coordinates is used. This is not the case when the

new ANCF models are used. No singularities are encountered because the joint constraint equations and the joint dependent variables are eliminated at a preprocessing stage.

4. In the case of simple geometry, one chain link can be modeled using one finite element. Therefore, the FFR coordinate reduction methods will not be advantageous, particularly if the high frequency axial modes need to be included in the model in order to capture the link tension forces. Furthermore, in tracked vehicle applications, the contact forces have very high frequency contents that can be comparable to the frequencies that results from the elastic forces.

Because of these reasons, the large deformation ANCF finite elements can be effectively used to efficiently solve small deformation problems. ANCF finite elements allow for implementing small deformation elastic forces models as described in the following section.

7. SMALL DEFORMATION ANCF ELASTIC FORCE MODEL

In this section, a simple force model, which can be used in the analysis of small deformation based on a three-dimensional ANCF Euler-Bernoulli beam, is introduced. The developed force model accounts for the coupling between bending and axial deformations. The model can be considered as a generalization of the two-dimensional force model developed by Berzeri et al (2001). Despite the simplicity of the proposed force model, it accounts for the elastic nonlinearity in the strain-displacement relationship.

7.1 Generalized Elastic Forces

The strain energy of the Euler-Bernoulli beam element can be written as a function of longitudinal strain ε_x and curvature κ as

$$U = \frac{1}{2}\int_0^l [EA\varepsilon_x{}^2 + EI\kappa^2]dx \ . \tag{8}$$

In the preceding equation, x is the longitudinal coordinate, l is the length of the element, E is the modulus of elasticity, A is the cross section area, and I is the second moment of area. The expression for the vector of elastic forces can be determined by differentiating the strain energy with respect to the ANCF coordinates as

$$\mathbf{Q}_e = \left(\frac{\partial U}{\partial \mathbf{e}}\right)^{\mathrm{T}} = \int_0^l [EA\varepsilon_x \frac{\partial \varepsilon_x}{\partial \mathbf{e}} + EI\kappa \frac{\partial \kappa}{\partial \mathbf{e}}]dx \, . \tag{9}$$

In the computer implementation, it is possible to derive the expressions for the derivatives in Eq. 9 by means of a symbolic computer program, or to derive them analytically in order to minimize the number of mathematical operations. Closed form expressions for the derivatives of both the axial strain and the curvature can be written as (Gerstmayr and Shabana, 2006)

$$\left.\begin{aligned}
&\frac{\partial \varepsilon_x}{\partial \mathbf{e}} = \mathbf{S}_x^T \mathbf{r}_x, \qquad \frac{\partial k}{\partial e_i} = \frac{1}{g^2}(g\frac{\partial f}{\partial e_i} - f\frac{\partial g}{\partial e_i}),\\
&f = |\mathbf{r}_x \times \mathbf{r}_{xx}|, \qquad g = |\mathbf{r}_x|^3,\\
&\frac{\partial f}{\partial e_i} = ((\mathbf{r}_x \times \mathbf{r}_{xx})^{\mathrm{T}}(\mathbf{r}_x \times \mathbf{r}_{xx}))^{-1/2}((\mathbf{r}_x \times \mathbf{r}_{xx})^{\mathrm{T}}(\frac{\partial}{\partial e_i}\mathbf{r}_x \times \mathbf{r}_{xx} + \mathbf{r}_x \times \frac{\partial}{\partial e_i}\mathbf{r}_{xx})),\\
&\frac{\partial g}{\partial e_i} = 3(\mathbf{r}_x{}^{\mathrm{T}}\mathbf{r}_x)^{1/2}(\mathbf{r}_x \frac{\partial \mathbf{r}_x}{\partial e_i})
\end{aligned}\right\} \tag{10}$$

The computation of these complex expressions can be time consuming, especially, for models containing a large number of elements. Berzeri et al (2001) introduced a simple model for the elastic forces of the planar Euler-Bernoulli beam element. Their model can be extended to the spatial Euler-Bernoulli beam element assuming small longitudinal deformation, which is the case for the steel track links used in the chains of the tracked vehicle model considered in this investigation. The expression for the elastic forces due to longitudinal forces can be written as

$$\mathbf{Q}_{e,l} = \int_0^l EA\varepsilon_x \frac{\partial \varepsilon_x}{\partial \mathbf{e}} dx = \int_0^l EA\varepsilon_x \mathbf{S}_x^T \mathbf{S}_x \mathbf{e} dx . \tag{11}$$

By assuming small variation of the strain over the length of the beam, the strain ε_x can be factored out from the expression of the elastic forces ,allowing writing the preceding equation as

$$\mathbf{Q}_{e,l} = EA\bar{\varepsilon}_x \int_0^l \mathbf{S}_x^T \mathbf{S}_x dx \mathbf{e} = \mathbf{K}_{e,l} \mathbf{e}, \tag{12}$$

where $\mathbf{K}_{e,l} = EA\bar{\varepsilon}_x \int_0^l \mathbf{S}_x^T \mathbf{S}_x dx$. The average axial strain can be simply calculated as $\bar{\varepsilon}_x = (d - l)/l$ where d is the current length of the beam.

The expression of the elastic forces due to bending can be written as

$$\mathbf{Q}_{e,t} = \int_0^l EI\kappa \frac{\partial \kappa}{\partial \mathbf{e}} dx . \tag{13}$$

In the case of small longitudinal deformation, the curvature can be defined as $|\mathbf{r}_{xx}|$. Hence, the transverse elastic forces can be written as

$$\mathbf{Q}_{e,t} = EI \int_0^l \mathbf{S}_{xx}^T \mathbf{S}_{xx} dx \mathbf{e} = \mathbf{K}_{e,t} \mathbf{e}, \tag{14}$$

where $\mathbf{K}_{e,t} = EI \int_0^l \mathbf{S}_{xx}^T \mathbf{S}_{xx} dx$.

Finally, the elastic force vector can be written as

$$\mathbf{Q}_e = (\mathbf{K}_{e,l} + \mathbf{K}_{e,t})\mathbf{e}, \tag{15}$$

where $\mathbf{K}_{e,l}$ and $\mathbf{K}_{e,t}$ are constant stiffness matrices associated with longitudinal and bending elastic forces, respectively.

7.2 Generalized Damping Forces

The internal damping characteristics of most known materials lead to energy dissipation when the materials are subjected to initial disturbances or shock loadings. Therefore, developing realistic flexible MBS models requires the inclusion of the effect of internal damping. One of the advantages of ANCF finite elements is the ability of capturing modes of deformations that cannot be captured using existing structural finite elements (Mohamed and Shabana, 2011). In some applications, some of these ANCF modes, which can have high frequencies, may not have significant effect on the solution. In such cases, explicit numerical integration schemes are forced to select very small time steps to capture the high frequencies. Therefore, for such applications, it is desirable to damp out these high frequency modes by using an appropriate visco-elastic constitutive model. This section introduces a suitable damping model that can be used with the simple elastic force model introduced in the previous section. The damping model introduced is also based on the assumption of small deformation.

The proposed visco-elastic model applies damping to the deformation associated with the gradient vector $\mathbf{r}_x$ and the curvature vector $\mathbf{r}_{ss}$ where s is the arc length. In order to properly define the deformation and avoid damping out rigid body displacement modes, a tangent frame can be used to define an orthogonal matrix using the vectors $\mathbf{r}_x$ and $\mathbf{r}_{ss}$ as $\mathbf{R} = \left[\frac{\mathbf{r}_x}{|\mathbf{r}_x|} \quad \frac{\mathbf{r}_x \times \mathbf{r}_{ss}}{|\mathbf{r}_x \times \mathbf{r}_{ss}|} \quad \frac{\mathbf{r}_{ss}}{|\mathbf{r}_{ss}|} \right]$. The power dissipated can be written as a function of the damping stress $\boldsymbol{\sigma}_d$ and the strain rate $\dot{\boldsymbol{\varepsilon}}$ as (Vallejo et al, 2005)

$$P_d = \frac{1}{2}\int_V \boldsymbol{\sigma}_d^{\mathrm{T}}\, \dot{\boldsymbol{\varepsilon}}\, dV . \tag{16}$$

Following a procedure similar to the one given in (Mohamed and Shabana, 2011; Mohamed, 2011), the power dissipated can be rewritten in the case of the Euler-Bernoulli beam element as

$$P_d = \frac{1}{2}\int_0^l \boldsymbol{\sigma}_d^{\mathrm{T}} \begin{bmatrix} A & 0 \\ 0 & I \end{bmatrix} [\dot{\varepsilon}_x \;\; \dot{\kappa}] dx, \tag{17}$$

where $\dot{\varepsilon}_x$ and $\dot{\kappa}$ are the longitudinal strain rate and curvature rate. By differentiating the dissipated energy with respect to the absolute nodal velocities, the generalized damping force can be written as

$$\mathbf{Q}_{\mathrm{d}} = \int_0^l (A(\frac{\nu_1 \dot{\varepsilon}_x}{1+2\varepsilon_x})\frac{\partial \varepsilon_x}{\partial \mathbf{e}} + I\nu_2 \dot{\kappa}\frac{\partial \kappa}{\partial \mathbf{e}})dx, \tag{18}$$

where ν_1 and ν_2 are two damping constants.

Using the assumption of small variation of the strain over the length, both the longitudinal strain and strain rate can be assumed constant through the length. Hence, the longitudinal damping force can be written as

$$\mathbf{Q}_{\mathrm{d,l}} = A\frac{\nu_1 \dot{\varepsilon}_x}{1+2\varepsilon_x}\int_0^l \mathbf{S}_x{}^{\mathrm{T}}\mathbf{S}_x \mathbf{e}\, dx = \mathbf{K}_{d,l}\mathbf{e} \tag{19}$$

where, $\mathbf{K}_{d,l} = A\left(\nu_1 \dot{\varepsilon}_x / \left(1+2\varepsilon_x\right)\right)\int_0^l \mathbf{S}_x{}^{\mathrm{T}}\mathbf{S}_x dx$. Using the same assumption, the curvature and curvature rate can be assumed constant through the length. Therefore, the transverse damping force can be written as

$$\mathbf{Q}_{\mathrm{d,l}} = I\frac{\nu_2 \dot{k}}{k}\int_0^l \mathbf{S}_{xx}{}^{\mathrm{T}}\mathbf{S}_{xx}\mathbf{e}\, dx = \mathbf{K}_{dtl}\mathbf{e}, \tag{20}$$

where. $\mathbf{K}_{d,t} = I\left(\nu_2 \dot{k}/k\right)\int_0^l \mathbf{S}_{xx}{}^{\mathrm{T}}\mathbf{S}_{xx}\mathbf{e}dx$. Then, the generalized internal damping force vector can be written as

$$\mathbf{Q}_d = (\mathbf{K}_{d,l}(\mathbf{e},\dot{\mathbf{e}}) + \mathbf{K}_{d,t}(\mathbf{e},\dot{\mathbf{e}}))\mathbf{e} \tag{21}$$

These generalized damping forces can be introduced to the ANCF element equations. The generalized damping forces associated with the ANCF Cholesky coordinates can also be obtained using the Cholesky transformation.

8. NUMERICAL RESULTS

A flexible-link chain three-dimensional tracked vehicle example is used in this section to demonstrate the implementation of the concepts discussed in this paper. This example represents a complex system with large number of bodies connected by large number of revolute (pin) joints. Furthermore, the mathematical models of such vehicles represent a stiff numerical integration problem due to high frequencies of the contact forces. Such vehicle models can be used to test the robustness of the MBS algorithm developed.

8.1 Model Description

The tracked vehicle used is an armored personnel carrier that consists of a chassis and two track chains. Each track system consists of an idler, one sprocket, 5 road-wheels, and 64 track links. A schematic drawing of the selected tracked vehicle is shown in Fig. 9. Table 1 shows the inertia properties for all the tracked vehicle model components used in this simulation. The vehicle has a suspension system that consists of a road arm, placed between each road wheel and the chassis, and a shock absorber that consists of a spring and a damper connecting each road arm to the chassis. In order to control the tension of the two tracks, each idler is connected to the chassis through a tensioner. Table 2 shows the stiffness coefficients k and the damping coefficients c of the contact models, the suspension system, and the tensioner; as well as the friction coefficient μ of the contact models. Ideal pin joints are used to connect the road arms and the sprockets to the chassis, and the road-wheels to the road arms. The normal contact forces are

calculated based on a linear dissipative contact force model (Choi et al, 1998; Maqueda et al, 2010; Dufva et al, 2007).

The models discussed in this section are assumed to have flexible track links. The flexible links are defined as three-dimensional steel Euler-Bernoulli beam elements with a modulus of rigidity of 76.9 GPa, a Young's modulus of 200 GPa, and a mass density of 7800 kg/m^3. The flexible chain links are connected to each other using ANCF ideal compliant pin joints, which define a linear ANCF mesh. As previously mentioned, one of the advantages of using this ANCF definition of joints is having linear joint constraints which allow for the elimination of the dependent joint variables at a preprocessing stage. As a result, this procedure avoids the computational cost required to formulate the nonlinear pin joint constraint equations at the position, velocity, and acceleration levels. In the case of the tracked vehicle used in this study, the proposed approach allows for the elimination of 126 pin joints and 630 highly nonlinear constraint equations at a preprocessing stage. In conventional MBS algorithms, this large number of highly nonlinear constraint equations must be satisfied at position, velocity, and acceleration levels. If ANCF joints are used, all these constraints become linear and can be eliminated at a preprocessing stage.

Three different tracked vehicle models are used to demonstrate the effectiveness of using the ANCF linear ideal compliant joint model. In the first vehicle, the chain links are modeled as rigid bodies. In order to solve the singularity problem encountered in the case of closed chain (Nakanishi and Shabana, 1994), the first and last links of the chain are connected through a very stiff spring. The links of the second and third tracked vehicle models are modeled as flexible links connected using ANCF continuum-based joints. The chain of the second model has a secondary joint by making a cut and using a very stiff spring to close the chain as in the case of

the rigid-link chains. In the case of the third model, on the other hand, an ANCF closed loop chain is used. The third model is used to demonstrate the fact that using the new linear ANCF joint model does not lead to any singularity problems as in the case of conventional MBS nonlinear joint algorithms. An explicit Adams-Bashforth predictor-corrector method was used for the numerical solution of the system differential equations.

8.2 Rigid Body Motion

The angular velocities of the two sprockets of all the three tracked vehicle models were specified to follow the pattern shown in Fig. 10. The response of the chassis to this input sprocket velocity is shown in Figs. 11-13. Figure 11 shows the forward velocity of the chassis. As expected, the velocity of the chassis follows the same pattern as the sprocket velocity. The results of Fig. 12 and 13 show the forward and vertical positions of the chassis center of mass. It can be noticed from the results presented in Fig. 14 that the chassis has 0.03m downward displacement as a consequence of an initial settlement of the suspension springs. These springs, in addition to the contact forces, deform under the effect of the weight of the vehicle components until equilibrium positions are reached. From the results presented in Figs. 11 to 13, it is clear that the rigid body motion results of the two flexible chain models are in a good agreement with the results of the rigid body model. Figure 14 shows the forward position of an arbitrarily selected point (end point of link 31). At the beginning of the simulation, this node is in contact with the ground. After that, the vehicle starts moving, and this point moves and it comes into contact with the idler. It continues moving until it comes again into contact with the ground. This motion is repeated as the vehicle continues to move forward. Figure 15 shows the motion trajectory of the same node defined in the chassis coordinate system.

8.3 Forces and Deformations

In tracked vehicle dynamics, it is important to study the reaction forces at the pin joints. These forces can be used to further analyze the strain and stress state of the chain and determine whether or not the chain can sustain the forces without failure. Figures 16 and 17 show the joint constraint forces of the first joint (marked in Fig. 21) in the longitudinal and the vertical directions for the rigid and ANCF joint models. One advantage of including the flexibility of the track links is to be able to calculate online the strains and stresses. The online computation of the track link deformation leads to a more realistic prediction of the system dynamics, this is due to a nature of the coupling between different displacement modes and simulation parameters. Figures 18 and 19 show the axial and transverse deformations of the first link of the right chain at $t = 5s$. In these figures, the deformation is magnified by a factor of 10^5. The deformation of this link was calculated using a local tangent frame that has its longitudinal axis parallel to the first node position gradient vector. Figure 20 shows the axial stress of the right track chain at $t = 5s$, while Fig. 21 shows the configuration of the chain at $t = 5s$. It is clear from the results of Figs. 20 and 21 that the chain span can be divided into three sections. First section, which is located before the sprocket and is directly affected by the sprocket forces, is the tight section which has the highest tension. The second section is the slack section located after the sprocket and has the lowest degree of tension. The third section is a transition section between the tight and slack sections of the chain.

While all the results of rigid body motion of the different models presented show good agreement, the computational time of the flexible model is almost four times the computational time of the rigid tracked vehicle model. This can be justified because of the high frequencies associated with the track link deformation. The presence of high frequencies can be confirmed by considering the number of function evaluations of the flexible and the rigid tracked vehicle

models. The ratio between the numbers of function evaluations for the rigid and flexible tracked vehicle is approximately $1:8.5$. Considering both the simulation time and the number of function evaluations, it can be concluded that using the new ANCF linear mesh in modeling the flexible link tracked vehicles leads to significant computational saving. This computational saving is the result of the elimination of the joint constraints and the corresponding dependent coordinates and Lagrange multipliers. Furthermore, numerical experimentation showed that when a low modulus of elasticity is used, flexible-link tracked vehicle models become more efficient than the rigid-link tracked vehicle model as the result of using the new ANCF finite element mesh.

9. SUMMARY AND CONCLUSIONS

In this paper, a new class of ideal compliant joints that account for the distributed inertia and elasticity is introduced and used to discuss fundamental issues related to the integration of computer aided design and analysis (I-CAD-A). Additional degrees of freedom are introduced in order to capture modes of deformation that cannot be captured using existing formulations that employ rigid triads or unit vectors to formulate the joint equations. The ideal compliant joints developed, while more general and capture more modes of displacements, can be, for the most part, formulated using linear algebraic equations. These linear connectivity conditions allow for the elimination of the dependent variables at a preprocessing stage, thereby significantly reducing the problem dimension and array storage needed. Consequently, the constraint equations are automatically satisfied at the position, velocity, and acceleration levels. Therefore, when using the proposed approach to model large scale chain systems, differences in computational efficiency between the augmented formulation and the recursive methods are eliminated, and the CPU times resulting from the use of the two formulations become similar regardless of the complexity of the system. Furthermore, the elimination of the joint constraint

equations and the associated dependent variables contribute to the solution of a fundamental *singularity problem* encountered in the analysis of closed loop chains and mechanisms, and there is no need to repeatedly change the chain or mechanism independent coordinates.

Using the concept of the ideal compliant joints, the fundamental problems that can be encountered when using computational geometry methods, can be explained. The concept of the knot multiplicity used in computational geometry methods is not suited for the formulation of ideal compliant joints that may require different degrees of continuity for different variables or elements of the gradient vector or require imposing constraints on the gradient vectors along directions that differ from the B-spline and NURBS coordinate lines. As explained in this paper, this issue is closely related to the inability of B-spline and NURBS to model *structural discontinuities*.

Another contribution of this paper is demonstrating that large deformation ANCF finite elements can be effective in solving small deformation problems. The necessity of using the new concepts developed in this paper in modeling complex systems is demonstrated using a heavily constrained tracked vehicle with flexible link chains. Without using the proposed approach modeling such a complex system with flexible links can be a challenging task. The analysis presented in this paper also demonstrates that adding significant model details does not necessarily imply increasing the complexity of the MBS algorithm. In fact, including significant details such as body flexibility and joint deformations can be accomplished using MBS algorithms that are much simpler than the algorithms currently used for rigid body system analysis.

Acknowledgment

This research was supported, in part, by the U.S. Army Tank-Automotive Research, Development and Engineering Center (TARDEC) (Contract No. W911NF-07-D-0001), and Computational Dynamics Inc.

REFERENCES

1. Abbas, L.K., Rui, X. and Hammoudi, Z.S., 2010, "Plate/Shell Element of Variable Thickness Based on the Absolute Nodal Coordinate Formulation", *Proceedings of the Institution of Mechanical Engineers, Part K: Journal of Multi-body Dynamics*, 224, pp. 127-141.
2. Bando, K., Yoshida, K. and Hori, K., 1991, "The Development of the Rubber Track for Small Size Bulldozers", *International Off-Highway & Powerplants Congress & Exposition, Milwaukee, WI*.
3. Berzeri, M., Campanelli, M. and Shabana, A.A., 2001, "Definition of the Elastic Forces in the Finite-Element Absolute Nodal Coordinate Formulation and the Floating Frame of Reference Formulation", *Multibody System Dynamics*, 5, pp. 21-54.
4. Choi, J.H., Lee, H.C. and Shabana, A.A., 1998, "Spatial Dynamics of Multibody Tracked vehicles, Part I: Contact Forces and Simulation Results", *Vehicle System Dynamics*, 29, pp. 27–49.
5. Choi, J.H., Lee, H.C. and Shabana, A.A., 1998, "Spatial Dynamics of Multibody Tracked vehicles, Part II: Contact Forces and Simulation Results", *Vehicle System Dynamics*, 29, pp. 113-137.
6. Dmitrochenko, O.N. and Pogorelov, D.Y., 2003, "Generalization of Plate Finite Elements for Absolute Nodal Coordinate Formulation", *Multibody System Dynamics*, 10, pp. 17-43.
7. Dufva, K.E., Sopanen, J.T. and Mikkola, A.M., 2005, "A Two-Dimensional Shear Deformable Beam Element Based on the Absolute Nodal Coordinate Formulation", *Journal of Sound and Vibration*, 280, pp.719–738.

8. Dufva, K., Kerkkänen, K. Maqueda, L.G., and Shabana, A.A., 2007, "Nonlinear Dynamics of Three-Dimensional Belt Drives Using the Finite-Element Method", *Nonlinear Dynamics,* 48, pp. 449-466.
9. Galaitsis, A.G., 1984, "A Model for Predicting Dynamic Track Loads in Military Vehicles", *Journal of Vibration, Acoustics, Stress, and Reliability in Design,* 106, pp. 286-291.
10. Gerstmayr, J. and Shabana, A.A., 2006, "Analysis of Thin Beams and Cables Using the Absolute Nodal Co-ordinate Formulation", *Nonlinear Dynamics,* 45, pp. 109-30.
11. Hamed, A.M., Shabana, A.A., Jayakumar, P. and Letherwood, M.D., 2011, "Non-Structural Geometric Discontinuities in Finite Element/Multibody System Analysis", *Nonlinear Dynamics,* 66, pp. 809-824.
12. Hughes, T.J.R., Cottrell, J.A. and Bazilevs, Y., 2005, "Isogeometric Analysis: CAD, Finite Elements, NURBS, Exact Geometry and Mesh Refinement", *Computer Methods in Applied Mechanics and Engineering*, 197, pp. 4104–412.
13. Korkealaakso, P., Mikkola, A., Rantalainen, T. and Rouvinen, A., 2009, "Description of Joint Constraints in the Floating Frame of Reference Formulation", *Proceedings of the Institution of Mechanical Engineers, Part K: Journal of Multi-body Dynamics*, 223, pp. 133-144.
14. Lan, P. and Shabana, A.A., 2010, "Integration of B-spline Geometry and ANCF Finite Element Analysis", *Nonlinear Dynamics*, 61, pp. 193-206.
15. Maqueda, L.G., Mohamed, A.A. and Shabana, A.A., 2010, "Use of General Nonlinear Material Models in Beam Problems: Application to Belts and Rubber Chains", *ASME Journal of Computational and Nonlinear Dynamics*, 5:2, pp. 849-859.

16. Mikkola, A., Shabana, A.A., Rebollo, C.S., and Octavio, J.R.J., 2013, "Comparison Between ANCF and B-spline Surfaces", *Multibody System Dynamics,* DOI 10.1007/s11044-013-9353-z.
17. Mohamed, A.A., 2011, "Visco-Elastic Nonlinear Constitutive Model for the Large Displacement Analysis of Multibody Systems", Thesis dissertation, University of Illinois at Chicago.
18. Mohamed, A.A. and Shabana, A.A., 2011, "Nonlinear Visco-Elastic Constitutive Model for Large Rotation Finite Element Formulation", *Multibody System Dynamics,* 26, pp. 57-79.
19. Nakanishi, T. and Shabana, A.A., 1994, "On the Numerical Solution of Tracked Vehicle Dynamic Equations", Nonlinear Dynamics, 6, pp. 391-417
20. Omar, M.A. and Shabana, A.A. 2001, "A Two-Dimensional Shear Deformation Beam for Large Rotation and Deformation", *Journal of Sound and Vibration*, 243, pp. 565-576.
21. Piegl, L. and Tiller,W. , 1997, *The NURBS Book*, Second ed., Springer, New York.
22. Schwab, A.L. and Meijaard, J.P., 2010, "Comparison of Three-Dimensional Flexible Beam Elements for Dynamic Analysis: Classical Finite Element Formulation and Absolute Nodal Coordinate Formulation", *Journal of Computational and Nonlinear Dynamics,* 5 (1), 011010-1 – 011010-10.
23. Shabana, A.A., 2012, *Computational Continuum Mechanics*, Cambridge University Press, Cambridge.
24. Shabana, A.A., 2010, "General Method for Modeling Slope Discontinuities and T-Sections using ANCF Gradient Deficient Finite Elements", *ASME Journal of Computational and Nonlinear Dynamics*, 6(2), 024502-1 - 024502-6

25. Shabana, A.A., 2014, *Dynamics of Multibody Systems*, Fourth Edition, Cambridge University Press, Cambridge.

26. Shabana, A. A., 2001, *Computational Dynamics*, Second edition, Wiley, New York.

27. Shabana, A.A., Hamed, A.M., Mohamed, A.A. , Jayakumar, P, and Letherwood, M.D., 2012, "Use of B-spline in the Finite Element Analysis: Comparison with ANCF Geometry", *Journal of Computational and Nonlinear Dynamics*, 7, pp. 81-88.

28. Shabana, A.A. and Mikkola, A.M., 2003, "Use of the Finite Element Absolute Nodal Coordinate Formulation in Modeling Slope Discontinuity", *ASME Journal for Mechanical Design*, 125(2), pp. 342–350.

29. Sugiyama, H., Escalona, J.L. and Shabana, A.A, 2003, "Formulation of Three-Dimensional Joint Constraints Using the Absolute Nodal Coordinates", *Nonlinear Dynamics*, 31, pp. 167-195.

30. Tian, Q., Chen, L.P., Zhang, Y.Q. and Yang, J.Z., 2009, "An Efficient Hybrid Method for Multibody Dynamics Simulation Based on Absolute Nodal Coordinate Formulation", *Journal of Computational and Nonlinear Dynamics*, 4, pp. 021009-1 - 021009-14.

31. Vallejo, D.G., Escalona, J.L., Mayo, J., and Dominguez, J., 2003, "Describing Rigid-Flexible Multibody Systems Using Absolute Coordinates", *Nonlinear Dynamics*, Vol. 34, pp. 75-94.

32. Vallejo, D.G., Valverde, J. and Domínguez, J., 2005, "An Internal Damping Model for the Absolute Nodal Coordinate Formulation", *Nonlinear Dynamics*, 42, pp. 347–369.

33. Yakoub, R.Y. and Shabana, A.A., 2001, "Three Dimensional Absolute Nodal Coordinate Formulation for Beam Elements: Implementation and Application", *ASME Journal for Mechanical Design*, 123, pp. 614–621.

Table 1. Tracked vehicle components inertia properties

Part	Mass (kg)	I_{XX} (kg m^2)	I_{YY} (kg m^2)	I_{ZZ} (kg m^2)	I_{XY}, I_{YZ}, I_{XZ} (kg m^2)
Chassis	5489.24	1786.92	10449.67	10721.22	0
Sprocket	436.67	13.87	12.22	12.22	0
Idler	429.57	14.70	12.55	12.55	0
Road Wheel	561.07	26.06	19.82	19.82	0
Road Arm	75.26	0.77	0.37	0.77	0
Track link	18.02	0.04	0.22	0.25	0

Table 2. Tracked vehicle contact and suspension parameters

Parameters	Sprocket-Track Contact	Roller-Track Contact	Ground-Track Contact	Suspension	Tensioner
k (N/m)	2×10^6	2×10^6	2×10^6	1×10^6	1×10^6
c (N·s/m)	5×10^3	5×10^3	5×10^3	1.5×10^4	1.4×10^4
μ	0.15	0.10	0.30	-	-

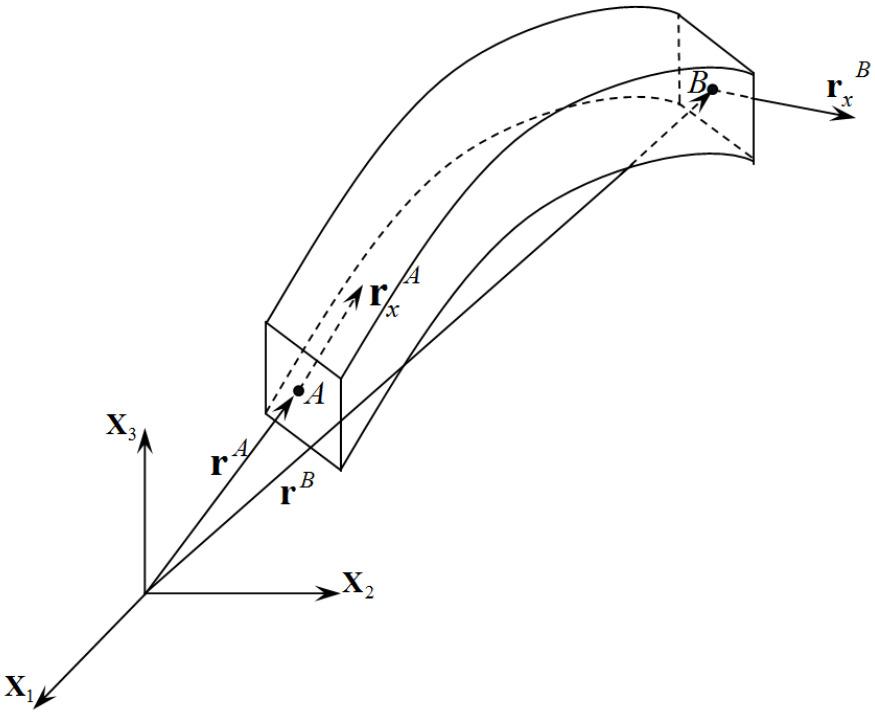

Figure 1. Euler-Bernoulli beam element

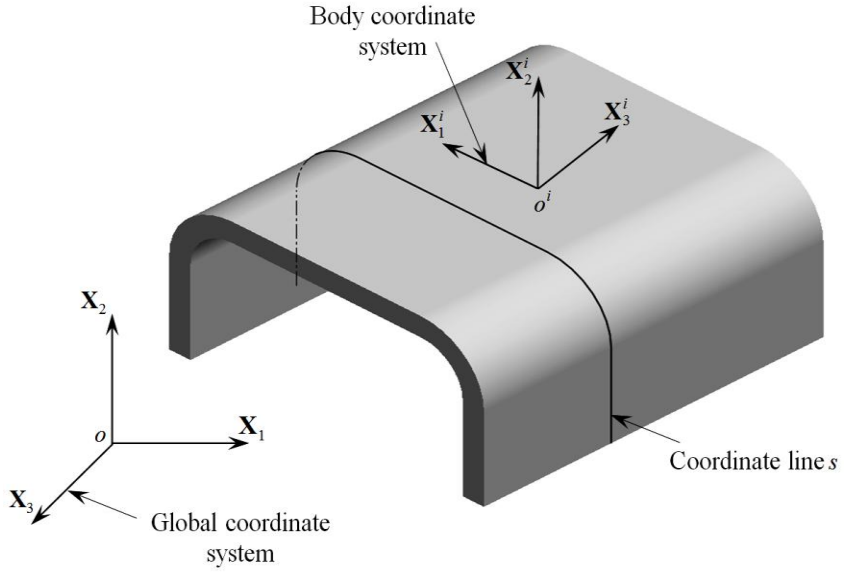

Figure 2. Structure without slope discontinuity

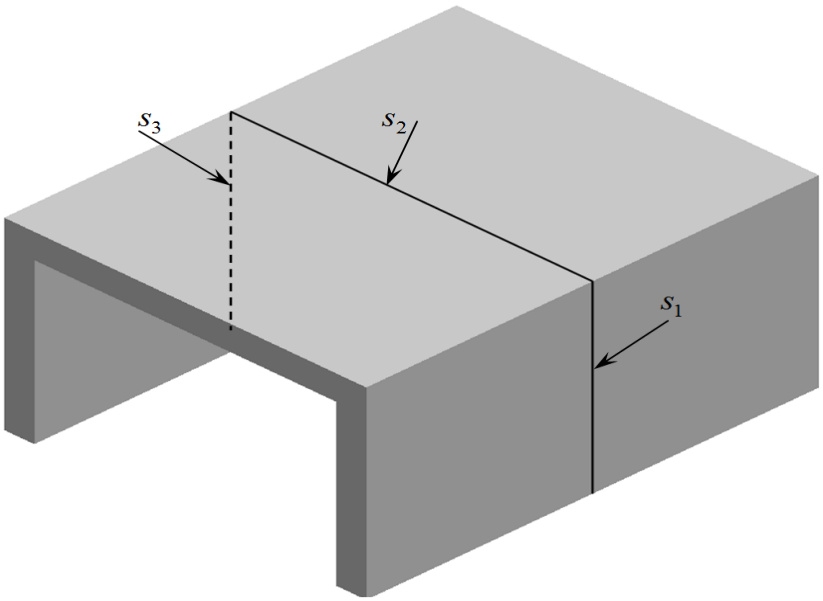

Figure 3. Structure with slope discontinuity

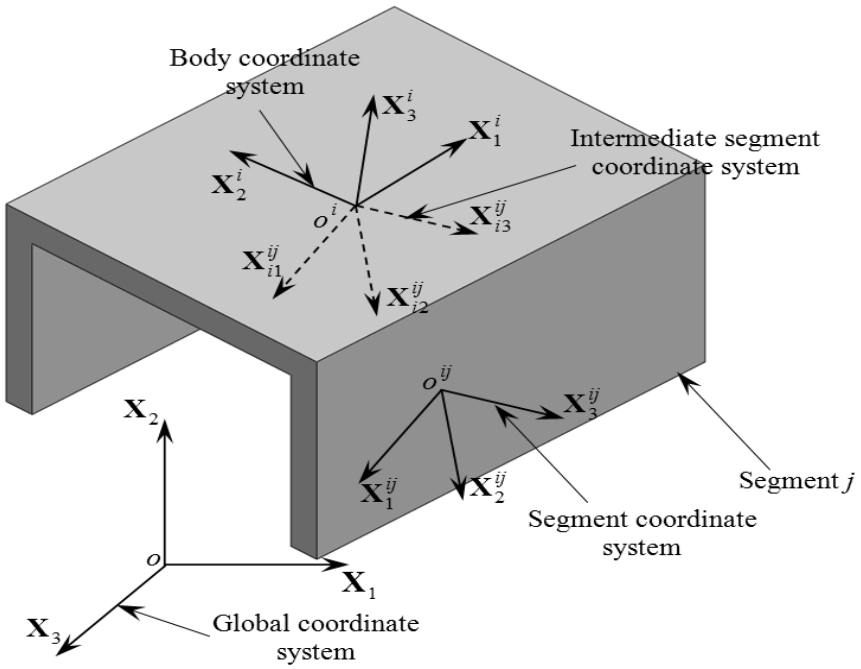

Figure. 4 Intermediate coordinate system

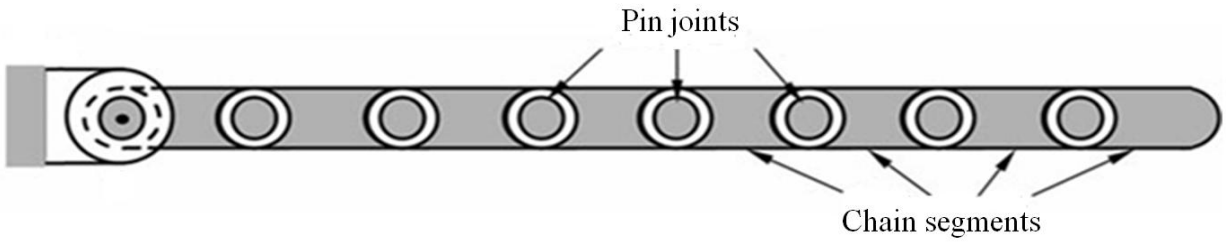

Figure 5. Eight-link chain

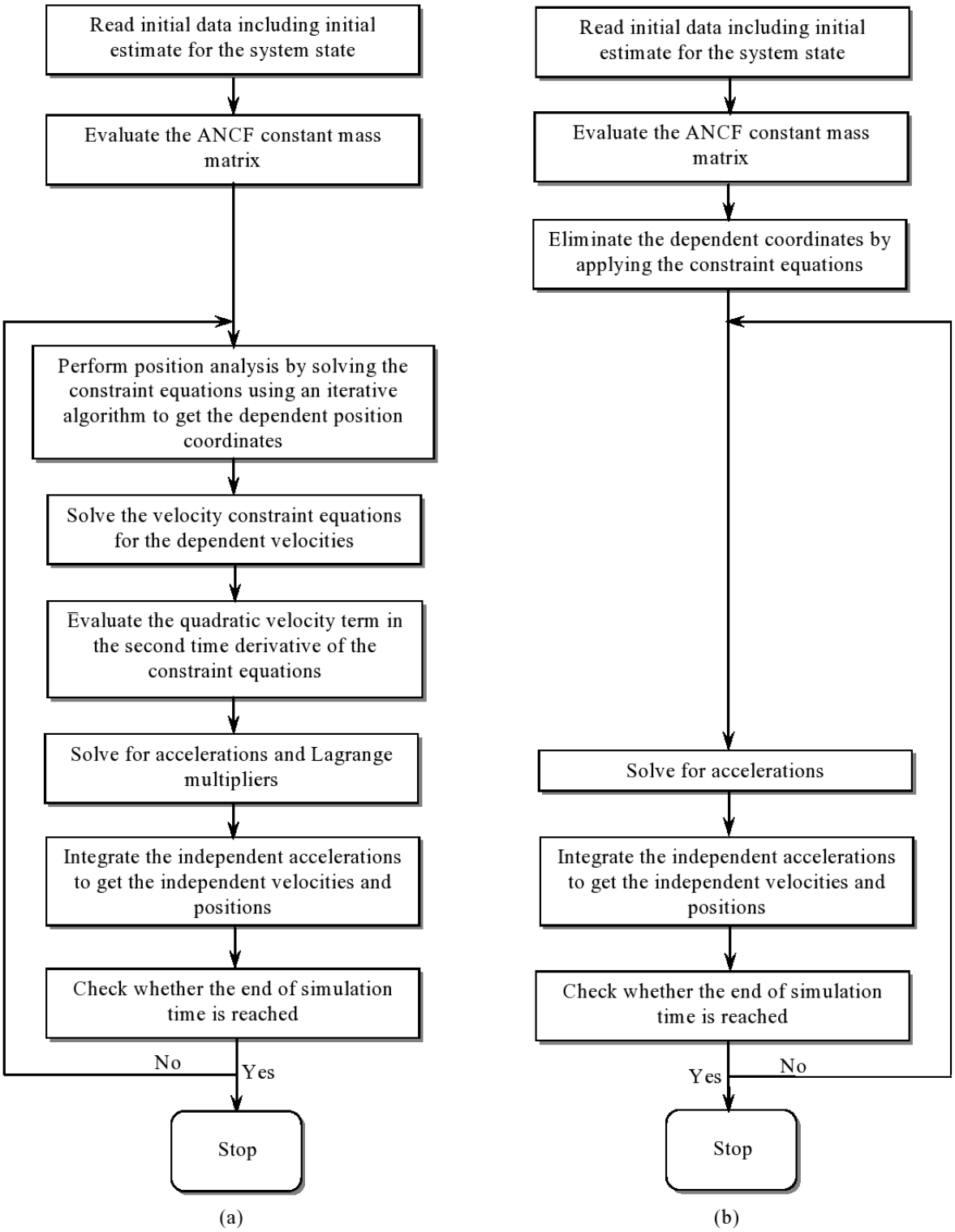

Figure 6. Algorithm flow chart
(a)Nonlinear constraints (b) New linear constraints

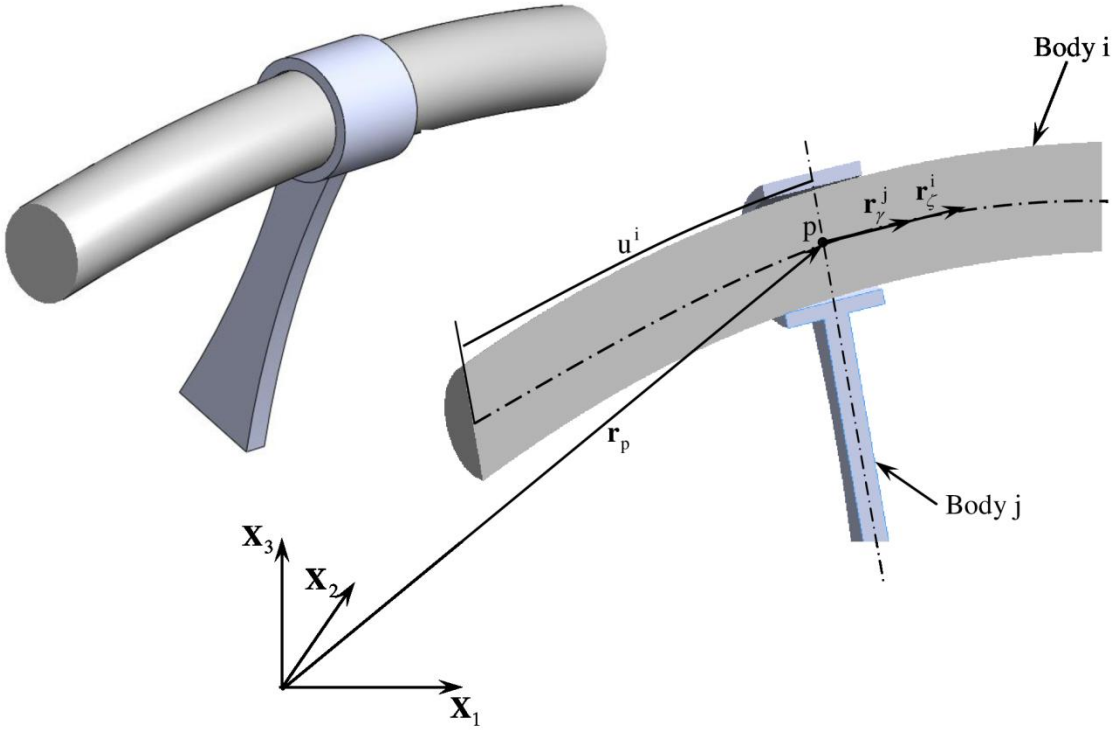

Figure 7. Sliding joint

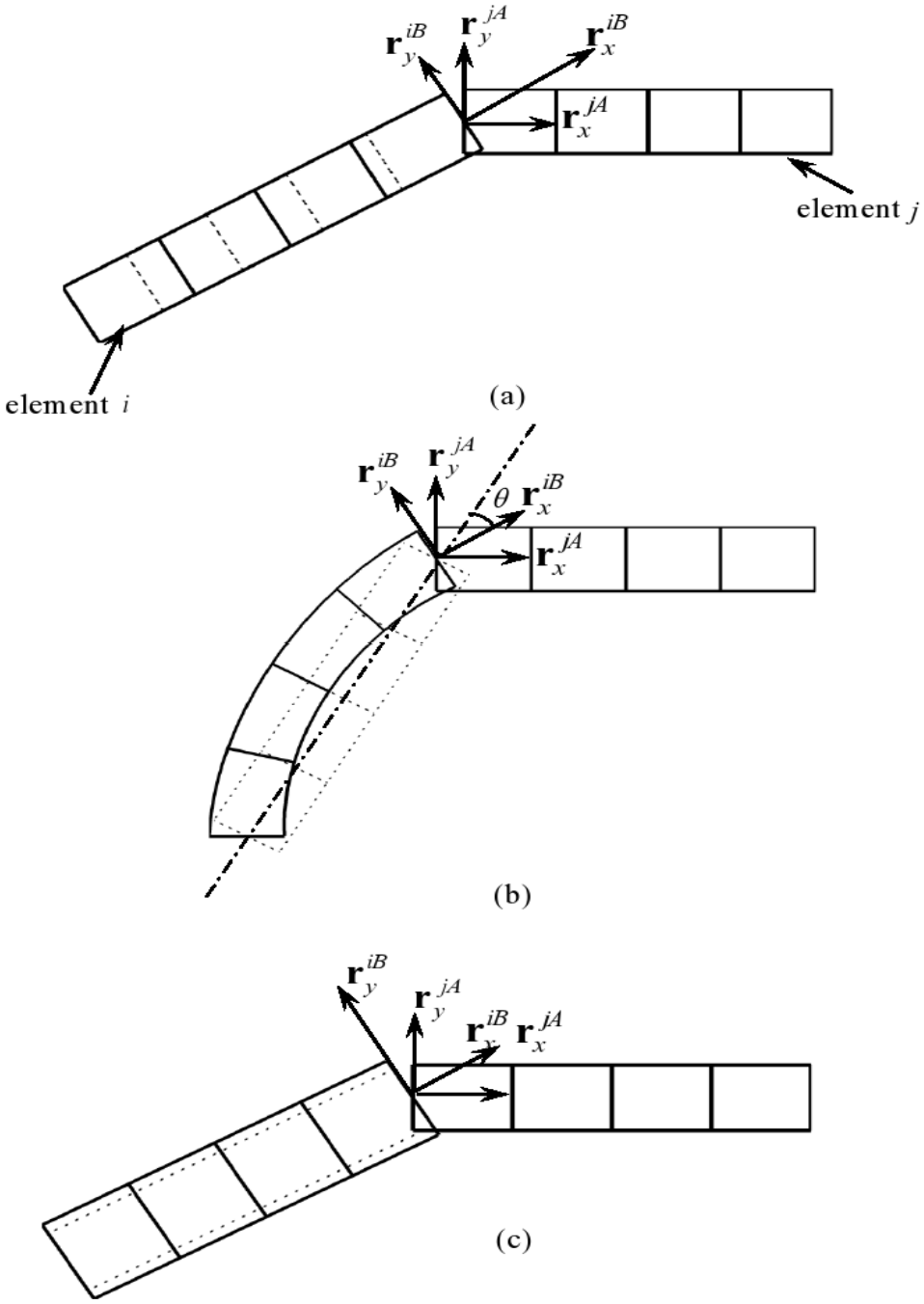

Figure 8. Deformation modes
(a) Tensile mode (b) Bending mode (c) Cross section deformation

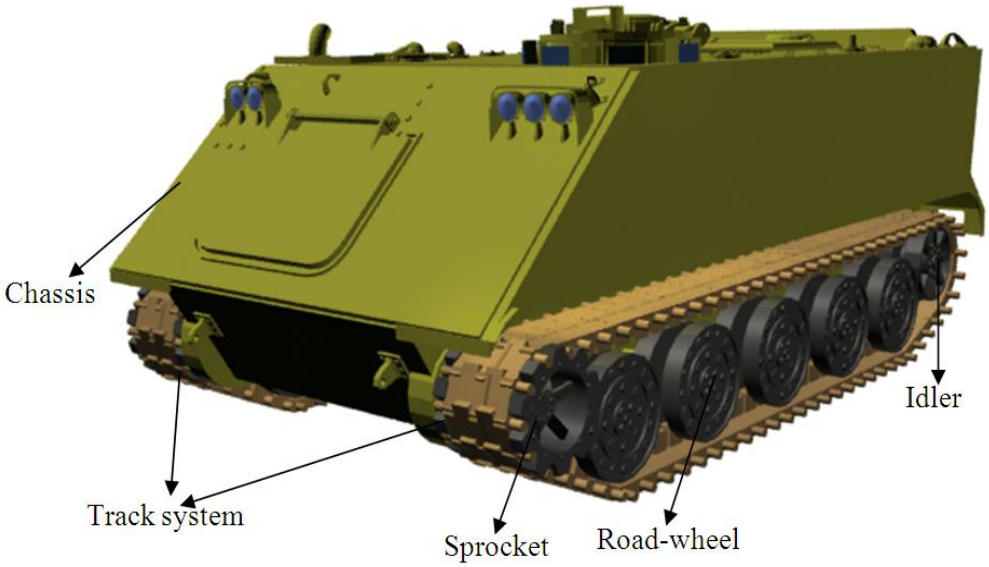

Figure 9. Tracked vehicle model

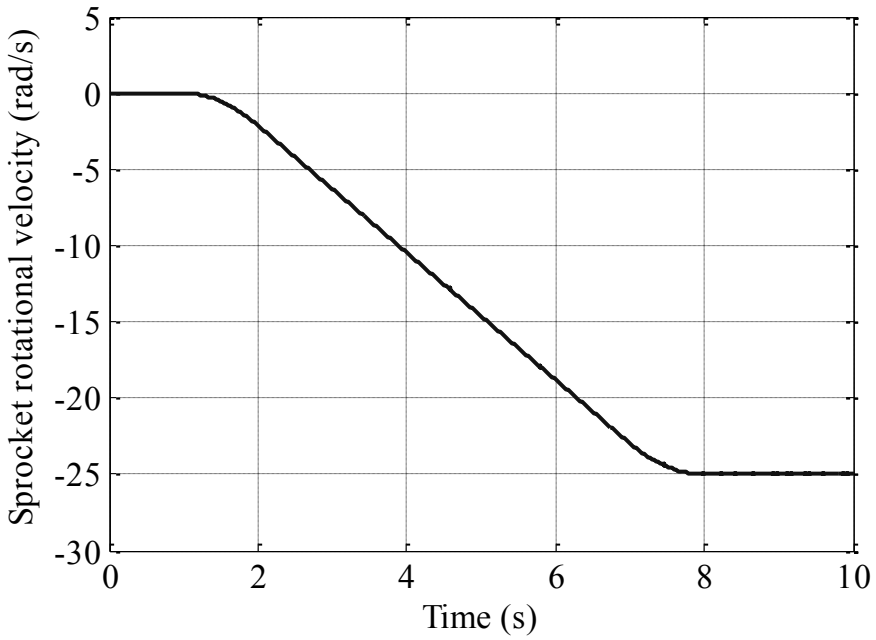

Figure 10. Sprocket rotational velocity

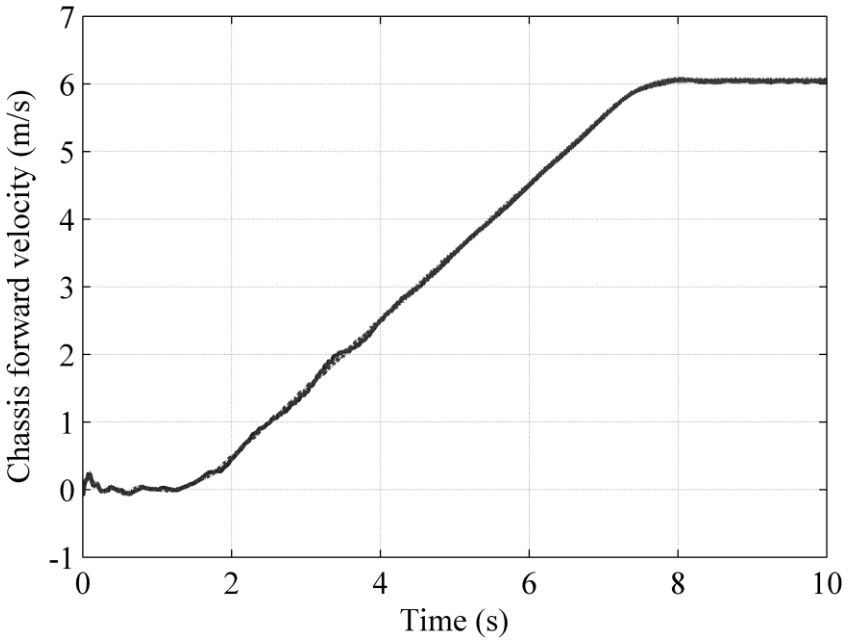

Figure 11. Chassis forward velocity
(-·-·-·- Rigid model, ——— Closed loop flexible model , ------- Open loop flexible model)

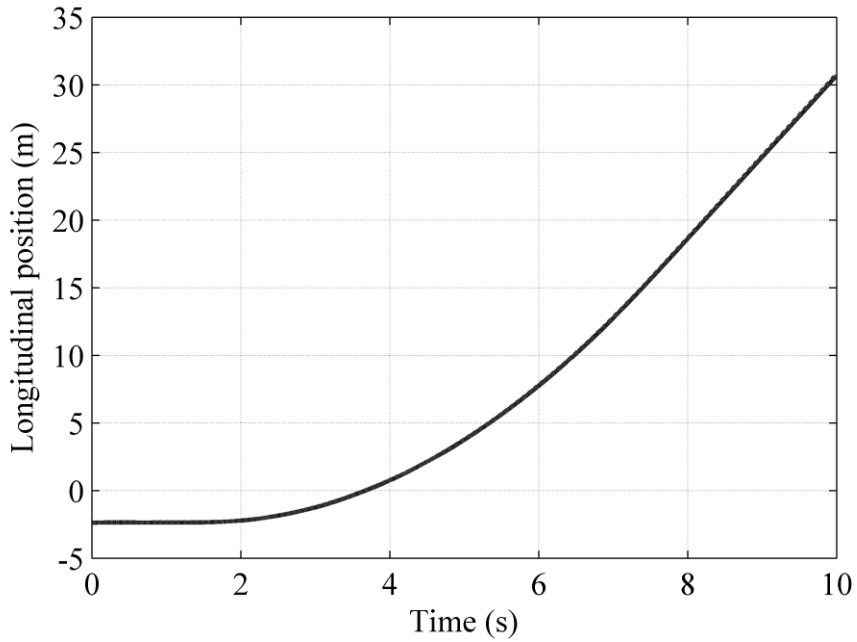

Figure 12. Forward displacement of the chassis
(-·-·-·- Rigid model, ——— Closed loop flexible model , ------- Open loop flexible model)

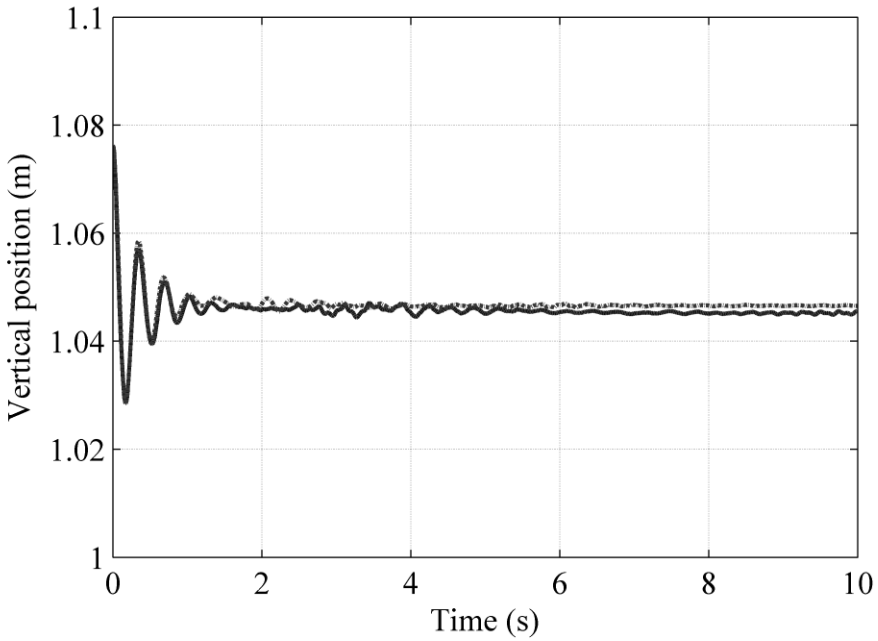

Figure 13. Vertical displacement of the chassis
(-·-·-·- Rigid model, ——— Closed loop flexible model , ------- Open loop flexible model)

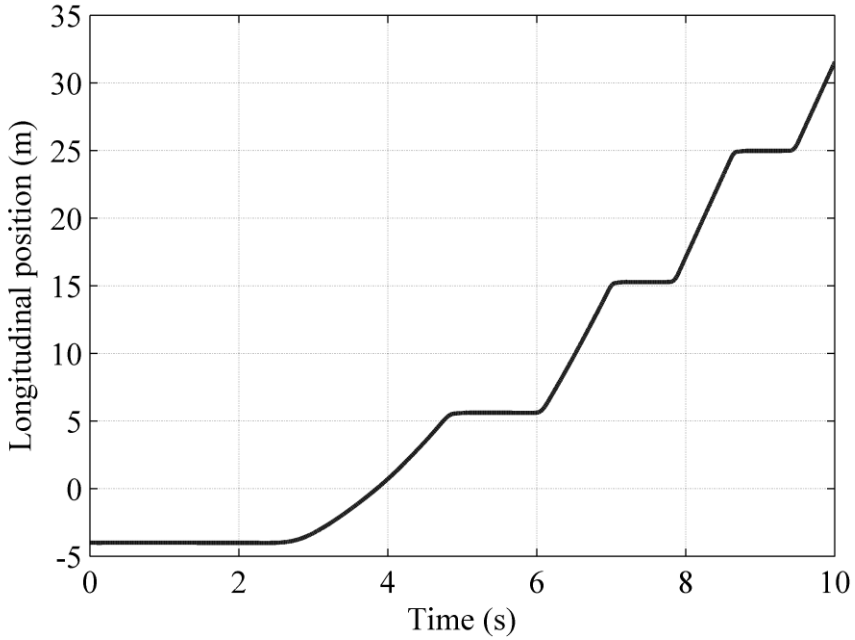

Figure 14. Node-32 forward position
(——— Rigid model, ------- Flexible models)

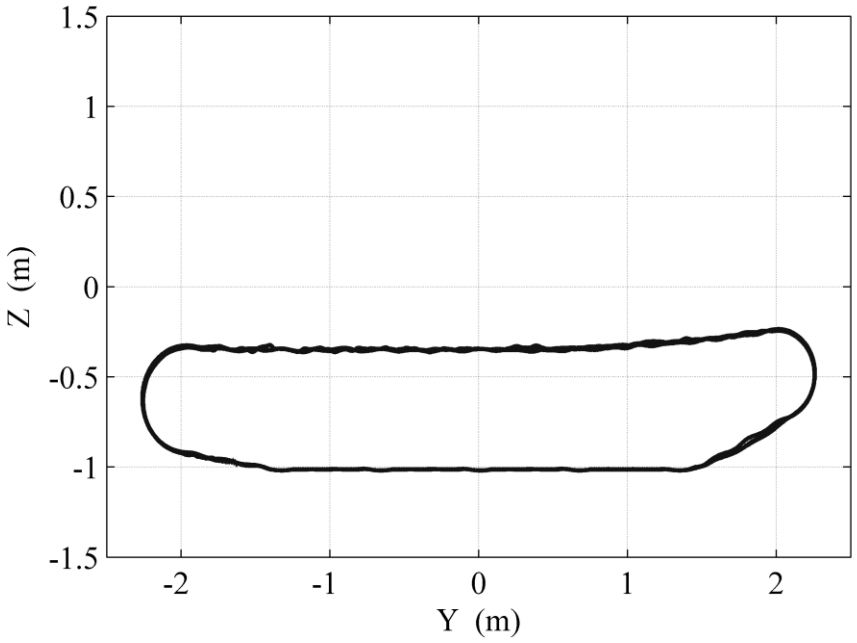

Figure 15. Motion trajectory of a flexible track link point

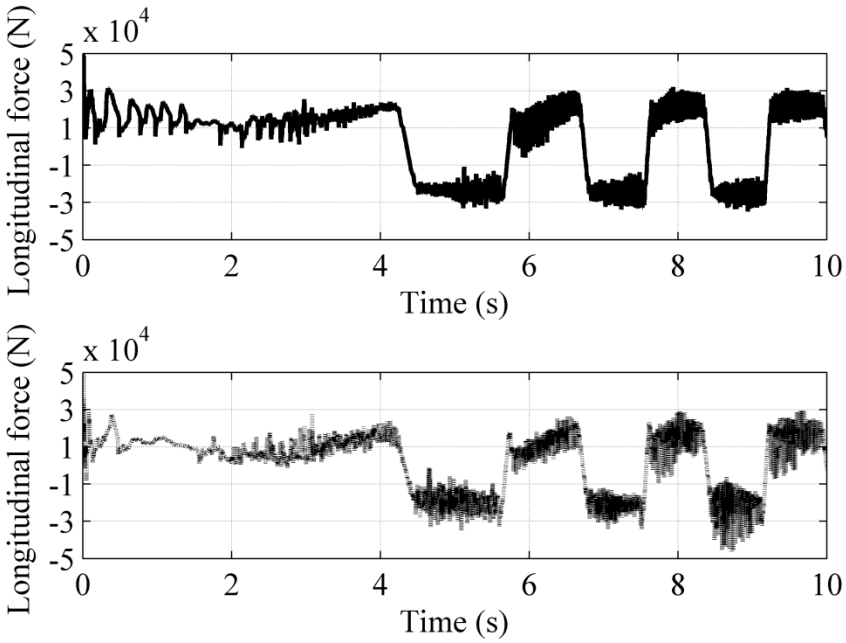

Figure 16. First joint longitudinal forces
(——— Rigid model, ------- Flexible models)

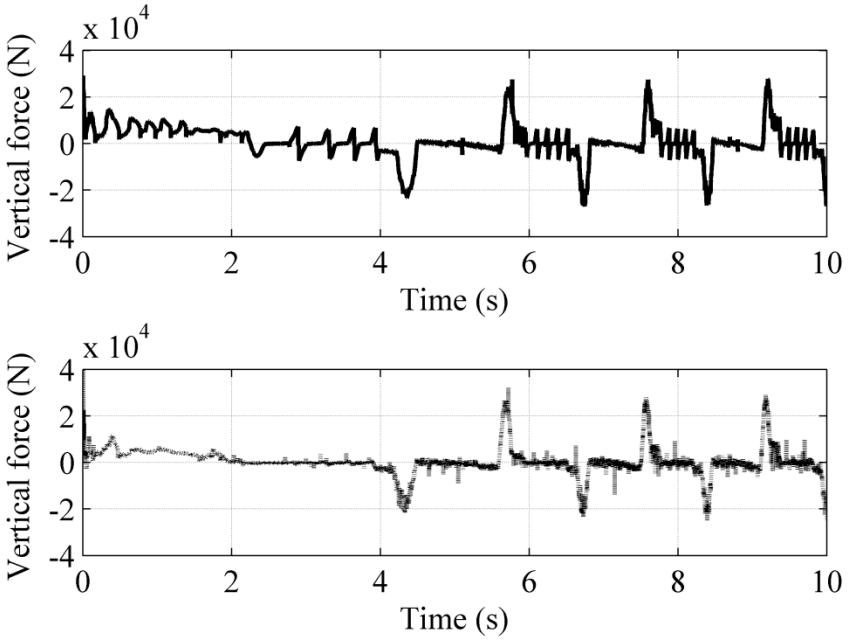

Figure 17. First joint vertical forces
(——— Rigid model, ------- Flexible models)

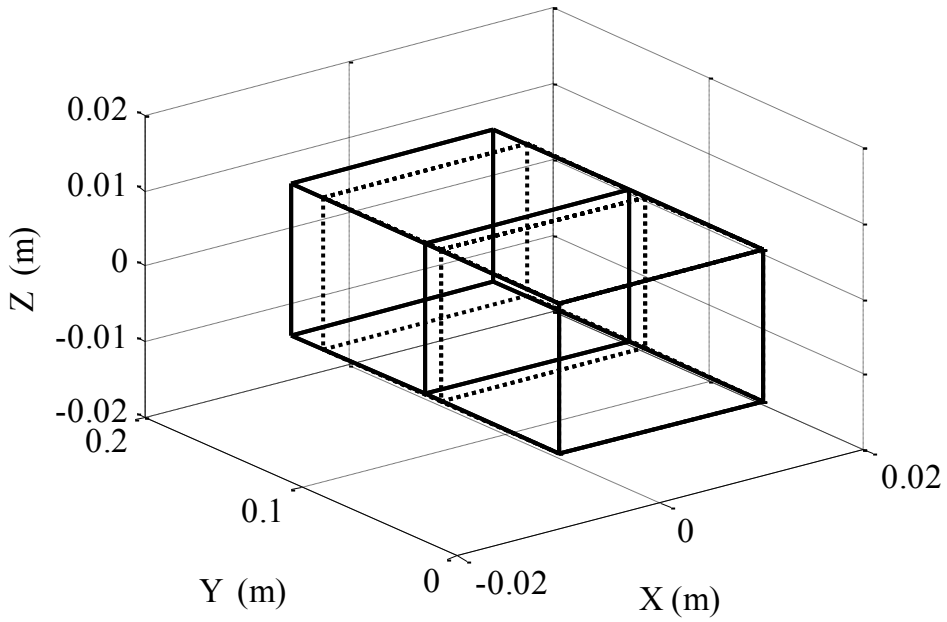

Figure 18. Axial deformation of first link of the right chain at $t = 5\text{s}$ magnified by a factor of 10^5
(------- Initial configuration, ——— Deformed configuration)

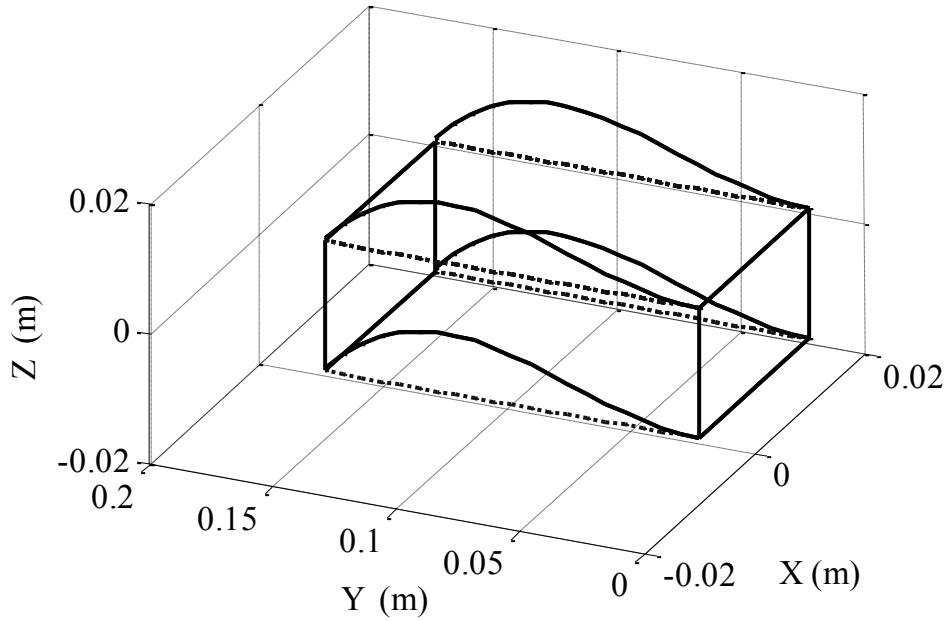

Figure 19. Transverse deformation of first link of the right chain at $t = 5\text{s}$ magnified by a factor of 10^5
(------- Initial configuration, —— Deformed configuration)

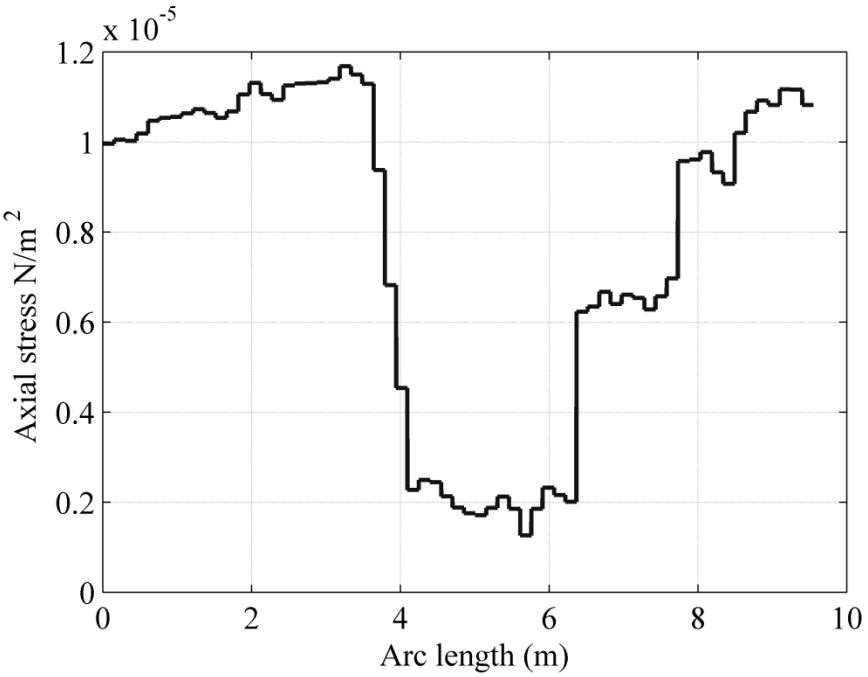

Figure 20. Right chain axial stress at $t = 5\text{s}$

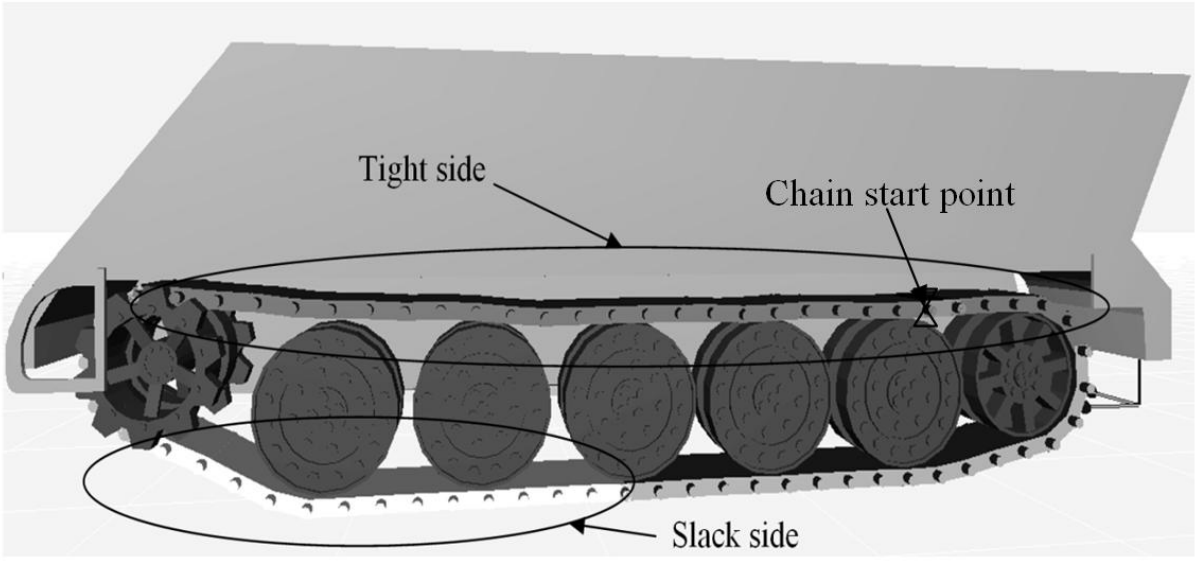

Figure 21. Right chain axial force distribution at $t = 5$s